asparagine residue within C-terminal transactivation domain of HIF-α (17). Asparagine hydroxylation is abrogated under hypoxic conditions (17), allowing HIF-α to recruit coactivators. Therefore, it has been speculated that both the prolyl and asparagine hydroxylases modulating HIF-α function may serve as oxygen sensors in the hypoxia signal transduction pathway (18).

As yet another determinant of cellular responsiveness to hypoxia, we have identified IPAS, a dominant negative regulator of HIF-α function (19). IPAS targets HIF-α subunits to form a complex lacking binding activity to the HRE and thereby impairs HIF target gene expression under hypoxic conditions. High expression of IPAS was found in the cornea, which correlates with low level of hypoxia-inducible VEGF expression and an avascular phenotype in this tissue. Thus, IPAS defines a novel mechanism of negative regulation of angiogenesis and tissue-specific control of responsiveness to hypoxic conditions (19). Interestingly, sequencing of the mouse IPAS genomic structure revealed that IPAS is a splicing variant of the HIF-3α locus (20).

An important physiological aspect of IPAS is its hypoxia-inducible expression. In tissues including brain, heart, lung, and skeletal muscle of mice, expression of IPAS mRNA is up-regulated following exposure to hypoxia, suggesting the presence of a negative feedback mode of regulation of hypoxia-inducible gene expression (19). Interestingly, such hypoxia-inducible expression of IPAS is supported at least in part by an alternative splicing mechanism that is observed exclusively under hypoxic conditions in these tissues (20).

Here we demonstrate that IPAS promoter activity is also induced by hypoxia. Functional analyses of the promoter region of IPAS/HIF-3α gene revealed an HRE mediating up-regulation of IPAS gene transcription under hypoxic conditions. HIF-1 binds to the *cis*-element and plays an essential role in transactivation of the IPAS gene. Thus, the IPAS-mediated negative feedback regulatory circuit in HIF-1-dependent gene regulation involves both hypoxia-dependent alterations in the splicing pattern of IPAS/HIF-3α transcripts as well as transcriptional activation of the IPAS-specific promoter.

EXPERIMENTAL PROCEDURES

Plasmids—For construction of a series of IPAS or HIF-3α promoter-driven luciferase reporter plasmids, various lengths of DNA fragments from the 5′-flanking region of IPAS exon 1a or HIF-3α exon 1 were amplified on mouse genomic DNA templates by PCR with flanking 5′-KpnI and 3′-NcoI enzyme restriction site using Platinum *pfx* DNA polymerase (Invitrogen). The PCR products were enzyme-digested then cloned into the KpnI-NcoI site of pGL3-Basic vector (Promega). Oligonucleotides corresponding to the sequence of the hypoxia-responsive 35-bp region of the IPAS promoter were synthesized and two or three copies of them were inserted in front of luciferase gene to generate reporter plasmids pIPAS/HRE 2x and pIPAS/HRE 3x, respectively. A hypoxia-inducible luciferase reporter containing three tandem repeat of HRE from the erythropoietin gene enhancer, pT81luc/HRE, HIF-1α, or Arnt expression plasmid pCMV4-HIF-1α or pCMV4-Arnt, respectively, and the expression plasmid pcDNA3 HIF-1α/1–396/VP16 encoding a constitutively active form of HIF-1α, have been described elsewhere (19, 21). To generate an IPAS/HIF-3α mini-gene plasmid, a genomic region containing exon 3, exon 4a, exon 4, and corresponding introns was cloned by PCR using bacterial artificial chromosome encompassing cognate mouse genomic fragment as a template and then ligated into pcDNA-3 vector (Invitrogen).

Cell Culture—Primary mouse brain endothelial cells (MBEC) were kindly supplied by Dr. Yihai Cao (Karolinska Institutet) and maintained in Ham's F-12 medium (Invitrogen) containing 10% fetal calf serum and antibiotics. Mouse hepatoma Hepa-1c1c7 cells were obtained from ATCC and cultured in α-minimum essential medium supplemented with 10% fetal calf serum and antibiotics. MBEC stably integrated with IPAS/HIF-3α mini-gene was established by lipocationic transfection and subsequent selection of the cells by the antibiotics G418 (Promega).

Isolation of Tissue Total RNA—Male C57Bl6 mice (8 weeks old) were exposed to either normoxic (21%) or hypoxic (6%) conditions for 6 h and then sacrificed by cervical dislocation, and the organs were removed. Total RNA was isolated from frozen tissues using RNA WIZ reagent (Ambion). All of the animal experiments were approved by the local animal research ethics committee of Institute of Medical Science, The University of Tokyo, Japan, and conducted according to their guidelines.

RNase Protection Assays—To generate the templates for an RNA probe, PCR was performed on mouse genomic DNA template using Platinum *pfx* DNA polymerase (Invitrogen) with the following primers; forward primer, 5′-TCTAGACCCTCCTC-CTTCTCGGGA-3′; reverse primer, 5′-AAGCTTCACGCGC-TGCAGCCCCAA-3′). The PCR product was digested with HindIII and XbaI and subcloned into the corresponding site of pcDNA3. The RNA probe was transcribed on the XbaI-digested templates by T7 RNA polymerase-based MAXI script *in vitro* transcription kit (Ambion) incorporating ^{32}P-labeled UTP. The full-length 202-bp riboprobe was separated and isolated on a denaturing polyacrylamide gel. The assay was performed using RPA III assay kit (Ambion). Briefly, the probe was coprecipitated with 50 μg of total RNA from the normoxic/hypoxic tissues, dissolved in hybridization buffer, and incubated at 42 °C for 18 h, followed by the digestion with the mixture of RNase A and T1. The protected RNA fragments were precipitated, denatured, then separated on an acrylamide gel, and visualized by autoradiography.

RT-PCR—For synthesis of first strand cDNA, 2 μg of DNase-treated total RNA from mouse tissues were reversely transcribed by Superscript II reverse transcriptase (Invitrogen) using oligo(dT)$_{18}$ primers, according to the manufacturer's protocol. PCR amplification using 1 μl of the first strand cDNA as a template was carried out in a total volume of 30 μl of mixture composed of 10 mM Tris-HCl (pH 8.3), 50 mM KCl, 1.5 mM $MgCl_2$, 200 μM dNTPs, 0.25 μM each of the sense and antisense primers, 1 unit of ExTaq DNA polymerase (TaKaRa, Japan). Amplification by 33 cycles of a step program (94 °C for 30 s, 51 °C for 30 s, and 72 °C for 1 min) was performed after 3 min of denaturing of the samples at 94 °C. The identities of the PCR products were confirmed by sequencing. Oligonucleotide PCR primers were as follows: exons 1a of IPAS, forward

(primer 1): 5′-AAGGGCGAGCATGGCGTTG-3′; exons 1 of HIF-3α, forward (primer 2): 5′-AGGACAGAGGGCCTTAGGCA-3′; exon 2 of IPAS/HIF-3α, reverse (primer 3): 5′-GGCGCATGATGGAGGCCTTG-3′.

Transient Transfection and Luciferase Assay—MBEC and Hepa1c1c7 cells were seeded in 6-well culture plate and transiently transfected with 1.0 μg of IPAS/HIF-3α promoter luciferase by the Lipofectamine reagent (Invitrogen). When indicated, HIF-1α, Arnt, or HIF-1α/1–396/VP16 expression plasmids were cointroduced into the cells. After 6 h of incubation, the culture medium was replaced with fresh medium and incubated for a further 24 h under either normoxic or hypoxic conditions, and then cellular extracts were prepared for luciferase activity measurement. pRL-SV40 vector (Promega) expressing *Renilla reniformis* luciferase under control by SV40 early enhancer/promoter was used as an internal control reporter for normalization of transfection efficiency.

Electrophoretic Mobility Shift Assay—Nuclear extracts were prepared from normoxic or hypoxic MBEC as described previously (19). Five micrograms of nuclear extract was incubated with ^{32}P-labeled W18 HRE probe (22) or an oligonucleotide probe encompassing the hypoxia-responsive region of the IPAS promoter (IPAS −834/−799) and its mutants (M1–M5) for 20 min on ice in a total volume of 30 μl containing 10 mM Tris-HCl (pH 7.8), 50 mM NaCl, 60 mM KCl, 1 mM $MgCl_2$, 1 mM EDTA, 5 mM dithiothreitol, 5% glycerol, 2% Ficoll, and 500 ng of poly(dI-dC) (GE Healthcare Bio-Sciences) and separated on 4% polyacrylamide gels at 200 V in 0.5× TBE (1× TBE: 89 mM Tris, 89 mM boric acid, 5 mM EDTA) buffer. The sequence of the sense strands of the oligonucleotides were as follows: 5′-CCCAAACCTGCATACGGAAGGAACACTGCTCCTTCACCCCTGT-3′ (IPAS −834/−799), 5′-CCCAAACCTGCATACGGAAGGAACACTGCTCCTTTTTCCCTGT-3′ (M1), 5′-CCCAAACCTGCATACGGAAGGAATTTTGCTCCTTCACCCCTGT-3′ (M2), 5′-CCCAAACCTGCATACGGAAGGAATTTTGCTCCTTTTTCCCTGT-3′ (M3), 5′-CCCAAACCTGCATACGGAAGGAACACTGCTCTTTCACCCCTGT-3′ (M4), and 5′-CCCAAACCTGCATACGGAAGGAACACTGCTCCTTCACTTTTGT-3′ (M5).

When indicated, 20 molar excess of unlabeled oligonucleotide or unspecific oligonucleotide was introduced to the reaction mixture for competition assay, and antibodies were used for induction of larger protein-DNA complexes.

Chromatin Immunoprecipitation (ChIP) Analysis—For the ChIP analysis, MBEC were cultured under either normoxic or hypoxic conditions for 6 h, washed once in PBS, and then incubated in PBS + 1% formaldehyde at room temperature for 10 min. The cells were washed with ice-cold PBS and then scraped into cold 100 mM Tris-HCl (pH 8.7), 10 mM dithiothreitol, incubated for 15 min at 30 °C, and subsequently pelleted at 4000 rpm for 5 min. The pellets were sequentially washed with cold PBS, Buffer I (0.25% Triton X-100, 10 mM EDTA, 0.5 mM EGTA, 10 mM HEPES, pH 6.5), and Buffer II (200 mM NaCl, 1 mM EDTA, 0.5 mM EGTA, 10 mM HEPES, pH 6.5). The pellets were then resuspended in lysis buffer (1% SDS, 10 mM EDTA, 50 mM Tris-HCl, pH 8.0) containing 1× Complete protease inhibitor mixture (Roche Applied Science) and thereafter sonicated until DNA was 500–700 bp in size. The samples were

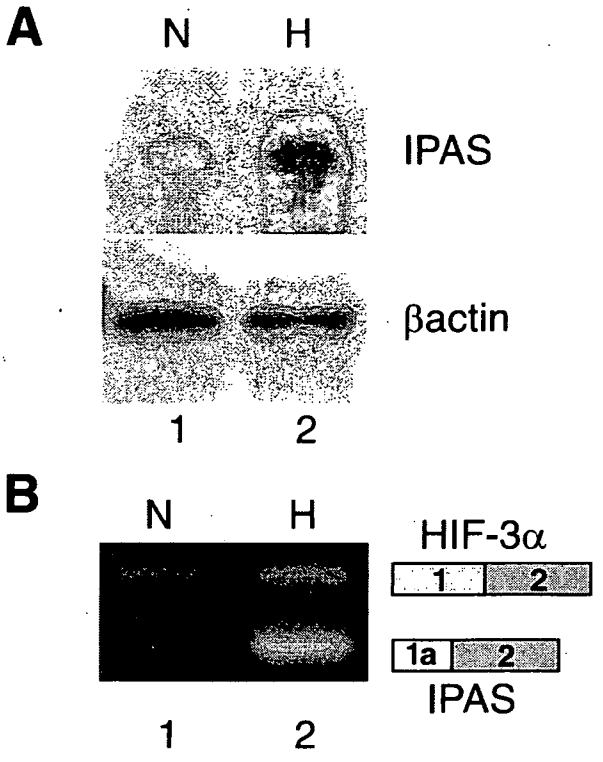

FIGURE 1. **Hypoxia increases IPAS gene transcription.** *A*, accumulation of the transcripts containing IPAS exon 1a in the heart of the mouse under hypoxic condition. The amount of the mRNA carrying IPAS exon 1a and its upstream sequence in the heart either from control mouse (maintained under normoxic conditions, *(N)* or mouse exposed to hypoxia *(H)* was determined by RNase protection assay. β-Actin mRNA levels were monitored as a reference for semi quantitative analysis. *B*, RT-PCR analysis of the expression level of IPAS or HIF-3α-specific transcript. The presence of either IPAS-specific transcript containing exon 1a-exon 2 junction or HIF-3α-specific transcript demonstrating exon 1-exon 2 connection in the same RNA samples as *A* was monitored by RT-PCR analysis using the exon-specific sets of primers.

diluted 1:10 in 1% Triton X-100, 2 mM EDTA, 150 mM NaCl, 20 mM Tris-HCl, pH 8.0, 1× Complete protease inhibitor mixture, and then incubated by rotation with 2 μg of sheared salmon sperm DNA, 6 μg of anti-human IgG antibodies (rabbit polyclonal, Abcam, Cambridge, UK) and 45 μl of 50% protein G-Sepharose slurry (GE Healthcare Bio-Sciences) for 2 h at 4 °C. Supernatant was collected by centrifugation at 3000 rpm for 15 s and incubated at 4 °C overnight by rotation with antibodies against HIF-1α (rabbit polyclonal, Novus Biologicals, Littleton, CO) or mouse IgG (rabbit polyclonal) as a negative control. 2 μg of sheared salmon sperm DNA. Thereafter 45 μl of 50% protein G-Sepharose slurry were then added and incubated by rotation for another 2 h at 4 °C. The Sepharose beads were collected at 3000 rpm for 15 s and sequentially washed for 15 min each under rotation with TSE I (0.1% SDS, 1% Triton X-100, 2 mM EDTA, 20 mM Tris-HCl, pH 8.1, 150 mM NaCl), TSE II (0.1% SDS, 1% Triton X-100, 2 mM EDTA, 20 mM Tris-HCl, pH 8.1, 500 mM NaCl), and Buffer III (0.25 M LiCl, 1% Nonidet P-40, 1% deoxycholate, 1 mM EDTA, 10 mM Tris-HCl, pH 8.1) at room temperature. The beads were washed three times with TE buffer followed by elution in 1% SDS, 0.1 M $NaHCO_3$ (3000 rpm, 15 s). The supernatants were incubated overnight at 65 °C, and DNA was purified using the PCR purification kit (Qiagen). The DNA was then used for 35 cycles of PCR together with

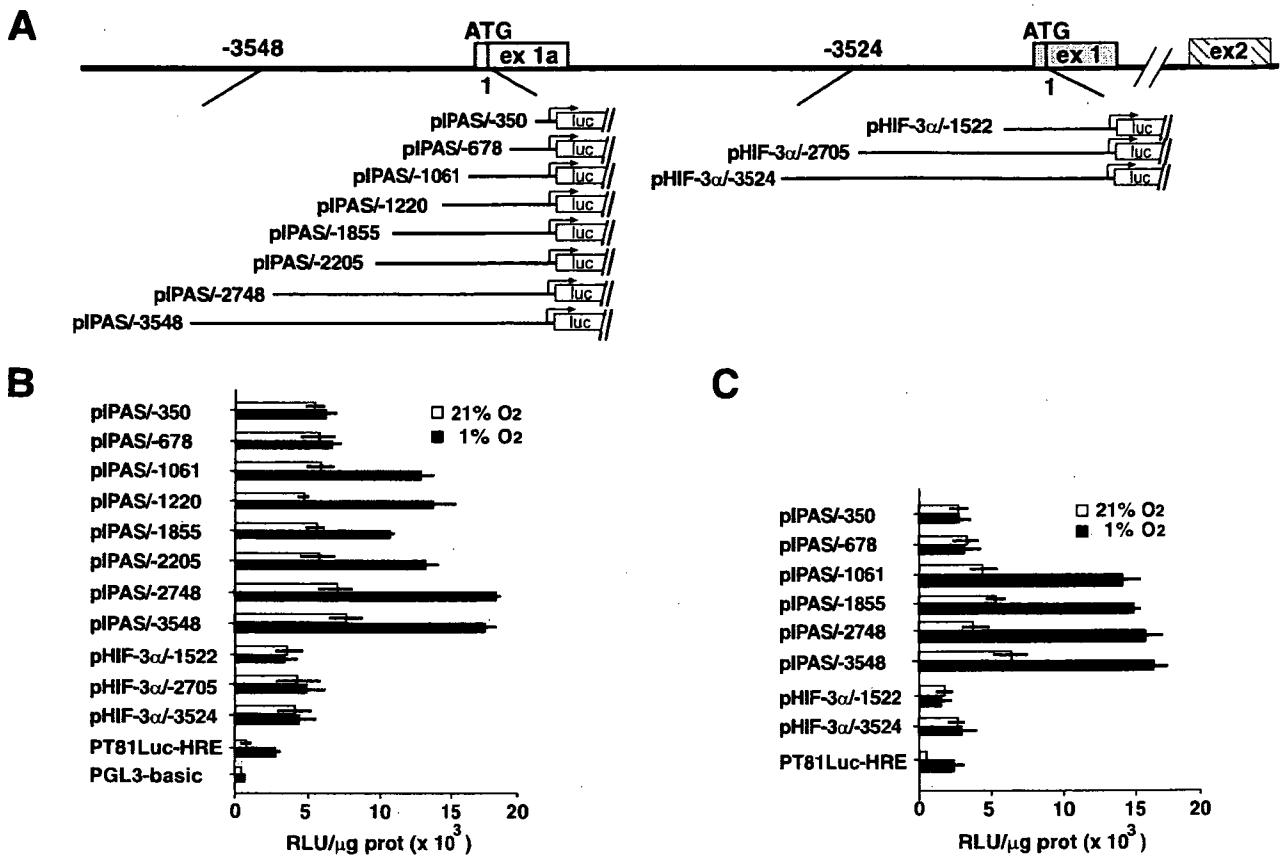

FIGURE 2. **Hypoxia responsiveness of the 5′-flanking region of IPAS exon 1a.** *A*, schematic representation of the IPAS or the HIF-3α promoter-driven luciferase constructs containing various length of 5′-flanking region of exon 1a or exon 1, respectively, of IPAS/HIF-3α gene. *B*, hypoxia inducibility of the IPAS promoter in MBEC. Reporter constructs were transiently transfected into MBEC as indicated, and after incubation of the cells either under normoxic (21% O_2) or hypoxic (1% O_2) conditions for 24 h, cellular luciferase activity was measured. HRE-driven luciferase plasmid was used as positive control for hypoxia-dependent luciferase expression. The results are shown by the means ± S.D. from three independent experiments. *RLU*, relative luciferase unit. *C*, activation of the IPAS promoter in mouse hepatoma cells under hypoxic condition. Luciferase plasmids were transiently transfected into Hepa-1c1c7 cells as indicated, and cellular luciferase activity under either normoxic (21% O_2) or hypoxic (1% O_2) conditions was determined. The experiments were performed in a triplication and the means ± S.D. of the results are shown.

primers flanking the putative HRE within the IPAS gene promoter: forward, CAATAAATCCATTTCTGCCGCA, and reverse, GAGAGGGCGTGGACACTAAGGA. Primers flanking the HRE of the VEGF gene promoter were used as a positive control: forward, AACAAGGGCCTCTGTCTGCCCA, and reverse, TTGTGGCACTGAGAACGGGGGT.

RESULTS

Hypoxia-dependent Up-regulation of IPAS Gene Transcription—To examine the involvement of the IPAS promoter in hypoxia-inducible IPAS gene expression, we performed RNase protection assays for determination of the level of mRNA containing exon 1a of the IPAS/HIF-3α gene. Total RNA extracted from the heart of mice either exposed to normoxic or hypoxic conditions was hybridized with an RNA probe encompassing IPAS exon 1a and its 138-base upstream sequence and then subjected to RNase digestion. The protected mRNA fragment corresponding to the transcript spanning from nt 1 to 62 of exon 1a was readily detected in RNA samples from normoxic mice, indicating basal transcriptional levels of the IPAS gene (Fig. 1*A*). In the heart from mice exposed to hypoxic conditions, the amount of the protected fragment containing IPAS exon 1a was clearly increased, whereas the level of β-actin mRNA was constant, demonstrating that the transcripts initiated upstream of IPAS exon 1a were specifically up-regulated by hypoxia (Fig. 1*A*). In excellent agreement with these observations, RT-PCR analysis using primers recognizing IPAS exon 1a and 2 showed up-regulation of the content of exon 1a in the transcripts isolated from hypoxic mouse heart tissue. Interestingly, the same RT-PCR analysis employing a primer pair specific for HIF-3α exon 1 showed only a modest increase of the transcript containing HIF-3α exon 1(Fig. 1*B*). Taken together, these data indicate that hypoxia specifically up-regulates transcription initiating in an upstream of IPAS exon 1a of the mouse *HIF-3α*.

Localization of the Sequence-mediating Hypoxia-dependent Activation of the IPAS Promoter—To further investigate the mechanism of hypoxia-dependent activation of the IPAS promoter, we generated and cloned into a luciferase expression vector a series of truncated fragments of the 5′-flanking region of the IPAS gene (Fig. 2*A*). MBEC were transiently transfected with these reporter plasmids and cultured either under normoxic (21% O_2) or hypoxic (1% O_2) conditions prior to monitoring of cellular luciferase activity (Fig. 2*B*). Cells transfected with pIPAS/−350 or with pIPAS/−678 luciferase reporter carrying 350- or 678-bp-long segments of the IPAS gene upstream

from the ATG in exon 1a, respectively, failed to show an increase of luciferase expression in response to hypoxia. Reporter constructs containing longer fragments of the IPAS promoter such as pIPAS/−1061, pIPAS/−1220, pIPAS/−1855, pIPAS/−2205, pIPAS/−2748, and pIPAS/−3548, produced similarly low levels of cellular luciferase activity under normoxic conditions. In contrast, under hypoxic conditions, these reporter plasmids showed 2–3-fold higher expression of luciferase, as compared with normoxic cells, indicating that a region mediating hypoxia-inducible IPAS gene transcription is localized between positions −678 and −1061 of the IPAS promoter (Fig. 2*B*). On the other hand, luciferase reporters fused to DNA fragments encompassing ~1.5, 2.7, and 3.5 kb upstream of HIF-3α exon 1 showed only basal levels of luciferase expression even following exposure to hypoxic conditions. Thus, in agreement with the lack of hypoxia-dependent generation of transcripts spanning HIF-3α exon 1, these data suggest that the HIF-3α promoter is not inducible by hypoxia (Fig. 2*B*). In support of this conclusion, experiments similarly conducted in a similar fashion in a different cell line, Hepa1c1c7 cells demonstrated the same location of the hypoxia-responsive region of the IPAS promoter, *i.e.* a location between nt −1061 and −678. Moreover, no hypoxia-dependent induction of the HIF-3α promoter was observed in these cells (Fig. 2*C*). Taken together, these data demonstrated that this sequence localized upstream of IPAS exon 1a mediates hypoxia-dependent induction of IPAS gene transcription.

Effect of HIF-1 on Promoter Activity of the IPAS Gene—To determine the involvement of HIF-1 in the hypoxia-dependent increase of IPAS promoter activity, the same set of luciferase reporters containing IPAS promoter sequences was cotransfected with a HIF-1α expression plasmid into MBEC. It has been described that overexpression of wild type HIF-1α by transient transfection induces HRE-regulated transcription to some extent even under normoxic conditions (23, 24), possibly because of saturation of endogenous pVHL levels and ensuing stabilization of the HIF-1α protein (9). Reporter gene activities by pIPAS/−350 and pIPAS/−678 were not influenced by coexpression of HIF-1α under normoxic culture conditions and not increased upon exposure to hypoxia (Fig. 3*A*). In contrast, activity of reporter constructs such as pIPAS/−1061, pIPAS/−1220, pIPAS/−1855, pIPAS/−2205, pIPAS/−2748, and pIPAS/−3548 were clearly augmented following coexpression of HIF-1α under normoxic conditions and further increased by hypoxia (Fig. 3*A*). On the other hand, overexpression of Arnt in the presence of the same panel of reporter plasmids (pIPAS/−1061, pIPAS/−1220, pIPAS/−1855, pIPAS/−2205, pIPAS/−2748, and pIPAS/−3548) in MBEC resulted neither in upregulation of basal luciferase activity under normoxic conditions nor in further hypoxia-dependent enhancement of the activity of the reporter genes (Fig. 3*B*). Taken together, IPAS promoter activity was increased by overexpression of HIF-1α, and the region mediating the effect of HIF-1α coincided with the locus responsible for hypoxia-inducible induction of the IPAS promoter.

Determination of the Functional Hypoxia Response Element in the IPAS Gene Promoter—To precisely map the *cis*-acting element mediating hypoxia-dependent IPAS promoter activation, we generated another set of luciferase reporters carrying different lengths of DNA fragments containing the 5′-flanking region of the IPAS gene and performed transient transfection assays normalized to SV40 early enhancer/promoter-generated *Renilla*-derived luciferase activities. MBEC transfected with pIPAS/−771 and pIPAS/−799 showed similar levels of modest luciferase activity either under normoxic or hypoxic conditions. In contrast, reporters pIPAS/−834 and pIPAS/−863 responded to hypoxia by expressing higher level of luciferase activity (Fig. 4*A*). These data suggested that an element of 35 bp between positions −834 and −799 of IPAS promoter is responsible for hypoxia-mediated activation of IPAS gene transcription. In an excellent agreement with these observations, pIPAS/−902, pIPAS/−964, pIPAS/−1023, and pIPAS/−1061, as well as the reporter constructs containing a longer fragment of IPAS promoter, pIPAS/−1220, showed the hypoxia-dependent induction response, whereas pIPAS/−678, pIPAS/−746 did not respond (Fig. 4*B*). In strong support of these observations, chimeric reporter constructs carrying two or three copies of

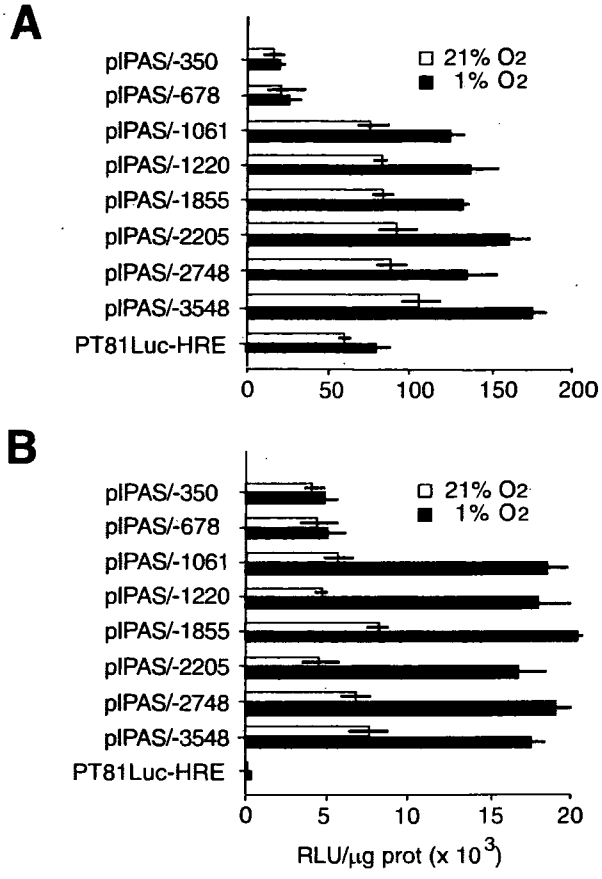

FIGURE 3. **Augmentation of the promoter activity of IPAS gene by coexpression of HIF-1α.** *A*, effect of HIF-1α on the IPAS promoter activity. IPAS promoter-driven and HRE-driven reporter plasmids were cointroduced with HIF-1α expression plasmid to MBEC by a transient transfection for 6 h. The cells were further incubated under either normoxic (21% O_2) or hypoxic (1% O_2) conditions for 24 h, and then cellular luciferase activity was determined. The experiments were repeated three times, and the means ± S.D. are shown as results. *B*, effect of overexpression of Arnt on the IPAS promoter activity. Expression plasmid for Arnt and a variety of IPAS promoter-luciferase plasmids were cotransfected into MBEC, and cellular luciferase activity after either normoxic (21% O_2) or hypoxic (1% O_2) culture was measured. The means ± S.D. of triplicated experiments are shown.

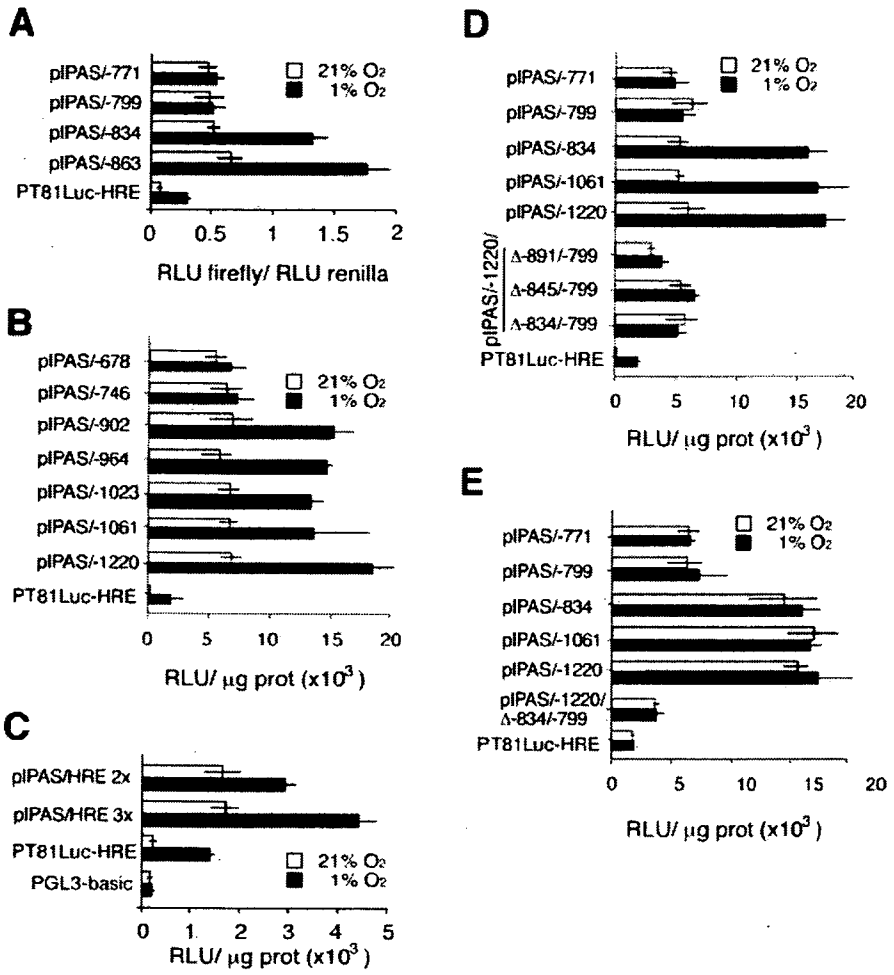

FIGURE 4. **Colocalization of the sequence responsible for hypoxia-dependent activation and for HIF-1α-mediated activation in the promoter region of IPAS gene.** *A* and *B*, determination of the hypoxia-responsive *cis*-element of the IPAS promoter. Luciferase constructs containing various length of 5′-flanking region of the IPAS gene were transiently transfected into MBEC, and cellular luciferase activity under either normoxic (21% O_2) or hypoxic (1% O_2) conditions was determined and normalized to coexpressed SV40 enhancer-driven *Renilla* luciferase activity. Luciferase plasmid under regulation by HRE was employed as a positive control for hypoxia-inducible gene expression. Relative values of IPAS promoter-luciferase activity (firefly luciferase) to *Renilla* luciferase activity in the cells (*A*) or to protein levels in the cellular lysate (*B*) were determined and shown by means ± S.D. *C*, isolated 35-bp hypoxia-responsive *cis*-element of the IPAS promoter confers induction response to hypoxic conditions. Two and three copies of the 35-bp hypoxia-responsive *cis*-element of IPAS promoter were placed in front of luciferase gene and transiently transfected into MBEC, and then cellular luciferase activity under either normoxic (21% O_2) or hypoxic (1% O_2) conditions was determined. HRE-driven luciferase plasmid and empty PGL3-basic luciferase plasmid were served as control for cellular luciferase expression. The results are shown by the means ± S.D. *D*, essential role of the 35-bp element in hypoxic induction of the IPAS promoter. Luciferase constructs containing various 5′-flanking region of the IPAS gene and their deletion mutants were transiently transfected into MBEC for determination of the hypoxic induction of the reporter activity. The results are shown by the means ± S.D. *E*, hypoxia response element in IPAS promoter is under regulation by HIF-1α. IPAS promoter-luciferase plasmids were cotransfected with an expression plasmid for the constitutively active form of HIF-1α into MBEC. After incubation of the cells under either normoxic (21% O_2) or hypoxic (1% O_2) conditions for 24 h, cellular luciferase activity was determined. The means ± S.D. of three independent experiments are shown as results.

this 35-bp region in front of the luciferase gene produced transcriptional response to hypoxia in a copy number-dependent manner (Fig. 4*C*). Moreover, removal of the sequences carrying the 35-bp region from hypoxia-responsive pIPAS/−1220, generating a reporter construct named pIPAS/−1220(Δ−891/−799), pIPAS/−1220(Δ−845/−799), and pIPAS/−1220(Δ−834/−799), resulted in loss of the hypoxia-dependent induction response (Fig. 4*D*). These data demonstrate that the 35-bp region of the IPAS promoter is critical for induction under hypoxic conditions. To further characterize the hypoxia-responsive 35-bp element of the IPAS promoter, we tested the effect of HIF-1α on the function of the region. To this end, we employed the expression plasmid for the constitutively active form of HIF-1α in reporter gene assays using IPAS promoter-luciferase constructs. As a constitutively active form of HIF-1α, we used a chimeric protein of truncated HIF-1α (lacking the degradation domain and endogenous transactivation function) fused to the activation domain of the viral transcription factor VP16: HIF-1α/1–396/VP16. This fusion protein has been shown to activate HRE-driven luciferase gene expression even under normoxic conditions, thus allowing us to test the direct effect of HIF-1α without the influence of other signaling pathways in the hypoxic cells (25). The IPAS promoter-luciferase reporter genes pIPAS/−834, pIPAS/−1061, and pIPAS/−1220 were induced by HIF-1α/1–396/VP16 in normoxia to levels comparable with those observed under hypoxic conditions. In contrast, neither pIPAS/−771 nor pIPAS/−799 responded to coexpression of HIF-1α/1–396/VP16, indicating that the 35-bp element between −834 and −799 is targeted for regulation by HIF-1α (Fig. 4*E*). In an excellent agreement with these data, the reporter construct lacking the 35-bp element, pIPAS/−1220(Δ−834/−799), failed to respond to constitutively active HIF-1α.

HIF-1 Binds to the Hypoxia-responsive cis-Element of the IPAS Promoter—To demonstrate binding of HIF-1 to the hypoxia-responsive region of the IPAS promoter, we performed EMSA using a labeled 35-bp oligonucleotide probe together with nuclear extracts of MBEC cultured either under normoxic or hypoxic conditions (Fig. 5). As shown in previous studies, when ^{32}P-labeled oligonucleotide corresponding to the HRE in the 3′enhancer of erythropoietin (Epo) gene was incubated with nuclear extracts of MBEC treated under hypoxic conditions, a more slowly migrating band was observed, indicating protein-HRE complex formation (Fig. 5, *lanes 3–7*). Competition by unlabeled oligonucleotides showed that formation of the DNA-protein com-

plex was specific for the HRE sequence (*lanes 4* and *5*), and induction of a supershift of the complex by anti-HIF-1α and -Arnt antibodies demonstrated that the complex is composed of HIF-1α and Arnt (*lanes 6* and *7*). Similarly, an oligonucleotide probe spanning nt −834 to −799 of the IPAS promoter formed a protein-DNA complex with nuclear extracts from hypoxic cells (*lanes 10–15*). The same unlabeled nucleotide sequence abolished complex formation, demonstrating the sequence specificity of the formed complex (*lane 11*). Moreover, addition of the antibody against HIF-1α shifted the complex to the more slowly migrating one, and an antibody for Arnt altered the amount of formed complex, indicating that HIF-1α and Arnt in the hypoxic nuclear extract generated the protein complex binding to the hypoxia-responsive element of the IPAS promoter (*lanes 14* and *15*). On the other hand, a 35-bp region next to the putative HRE of the IPAS promoter, *i.e.* a region spanning the promoter sequence −870 to −835, failed to generate any specific protein-DNA complexes even with the hypoxic nuclear extracts, indicating the absence of a HIF-1-binding site (HBS) at this region of the IPAS promoter (*lanes 17–20*). The hypoxia-responsive 35-bp element of the IPAS promoter contains three classical HBS-like motifs: the region from −810 to −805, −813 to −808, and from −821 to −816 (Fig. 6*A*, indicated by *arrows*). To determine the HIF-1-binding sequence of the IPAS promoter, we generated a panel of mutant 35-bp oligonucleotides in which adenine triplets substitute for half-sites of the HBS-like motifs (Fig. 6*A*) and performed EMSA using those mutants as probes. Oligonucleotide probes carrying consensus 18-nt Epo-HRE or wild type 35-bp HRE of the IPAS promoter formed protein-DNA complexes with the nuclear extracts from MBEC exposed to hypoxic conditions. Mutations of the proximal (−810 to −805 indicated by *box*) HBS-like motif, resulting in M1, M3, and M5 probes, diminished complex formation, whereas mutations of the distal (−821 to −816) HBS-like motif (M2 and M4 probes) did not influence the DNA binding activity in the hypoxic nuclear extract, demonstrating that HIF-1 binds to the proximal HBS-like motif in IPAS promoter located at positions −810 to −805 of the IPAS promoter (Fig. 6*B*). Finally, to directly test whether endogenous HIF-1α binds to the HREs of the IPAS gene promoter *in vivo*, we performed a ChIP assay using MBEC cultured under either normoxic or hypoxic conditions. VEGF represents a HIF-1α target gene with a well characterized HRE in its promoter region thus serving as a positive control. Following cross-linking, an anti-HIF-1α antibody was used to precipitate HIF-1α protein, and the amount of coprecipitated HRE-containing genomic DNA fragments of the IPAS and the VEGF promoter was assessed by PCR. Genomic DNA fragments prior to immunoprecipitation generated similar signals from hypoxic and normoxic MBEC with specific primer pairs either for the VEGF or for the IPAS promoter, indicating optimum sonication and equal input of genomic DNA (Fig. 7, *lanes 1* and *2*). When precipitated with control rabbit polyclonal antibodies, DNA fragments from both nor-

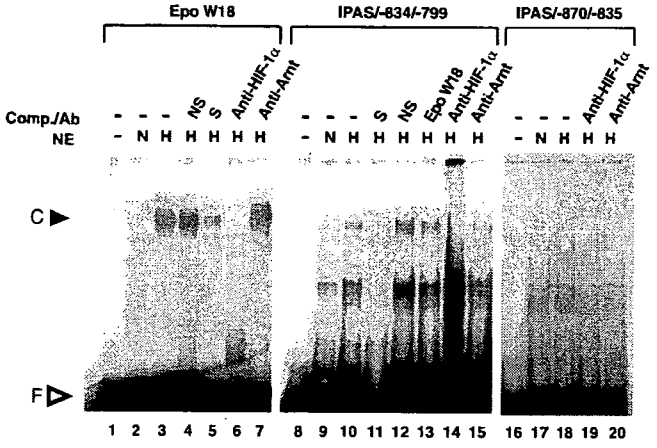

FIGURE 5. **HIF-1 binds to the hypoxia-responsive *cis*-element in the promoter region of IPAS gene.** Nuclear extracts (*NE*) from MBEC were prepared after incubation under either normoxic (*N*) or hypoxic (*H*) condition for 6 h. ^{32}P-Labeled oligonucleotide probes encompassing HRE in 3′-enhancer of erythropoietin gene (Epo W18), 35 bp between −834 and −799 nt upstream of the IPAS exon 1a (IPAS/−834/−799), and 28 bp between positions −870 and −835 of IPAS gene (IPAS/−870/−835) were mixed with the nuclear extracts, and the formed protein-DNA complexes were separated on 4% polyacrylamide gel. Molar excess of unlabeled Epo W18 or IPAS/−834/−799 oligonucleotide was used as a specific competitor (*S*), respectively, and unlabeled randomized 20-mer oligonucleotide was used for nonspecific competition (*NS*). Anti-HIF-1α or -Arnt antibody was employed for supershift experiments. *C*, DNA-protein complex; *F*, free probe.

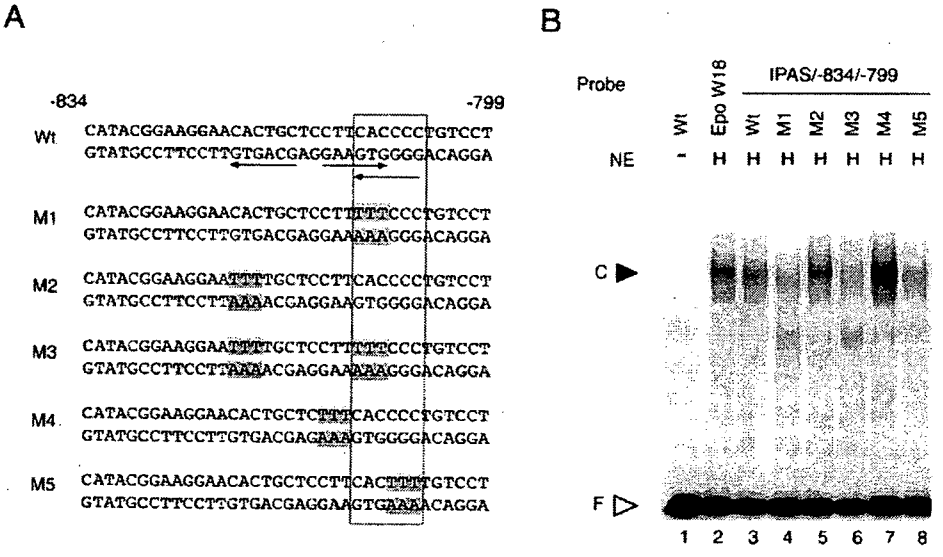

FIGURE 6. **Determination of HIF-1-binding site in the hypoxia response region of the IPAS promoter.** *A*, sequence of oligonucleotide probes corresponding to the hypoxia response 35-bp region of the IPAS promoter (*Wt*) and its various substitution mutants (M1–M5). The hypoxia response region of IPAS promoter contains classical HBS-like motifs (indicated by *arrows*). Substituted nucleotides in mutant probes are indicated by *shading*. *B*, proximal HBS-like motif is involved in HIF-1 binding to the IPAS promoter. Nuclear extracts (*NE*) from hypoxic MBEC was incubated with ^{32}P-labeled wild type (*Wt*) or mutant probes (M1–M5) as indicated in *A*, and protein-DNA complex formation was monitored by polyacrylamide gel electrophoresis. Epo W18 probe was used as positive control for HIF-1-DNA complex formation. *C*, DNA-protein complex; *F*, free probe.

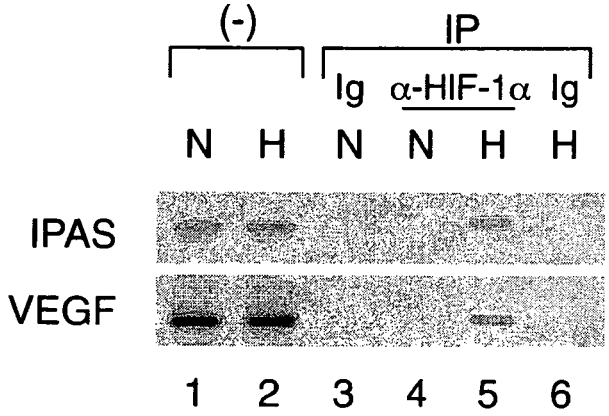

FIGURE 7. **HIF-1α binds to the hypoxia response region of the IPAS promoter *in vivo*.** ChIP assay using MBEC cultured under either normoxic (21% O_2, *N*) or hypoxic (1% O_2, *H*) conditions for 6 h. The cells were incubated with formaldehyde for cross-linking, and then DNA was extracted and immunoprecipitated (*IP*) with anti-HIF-1α antibody (α-HIF-1α) or rabbit polyclonal immunoglobulins (*Ig*). After reversal of cross-linking, DNA was recovered and used in PCR for 35 cycles. Primers flanking the hypoxia-responsive region of the IPAS promoter or the HRE of the VEGF gene enhancer were included in PCRs and generated a 103- or 163-bp product, respectively. For input, DNA from the extract prior to immunoprecipitation (*(−)*) was used.

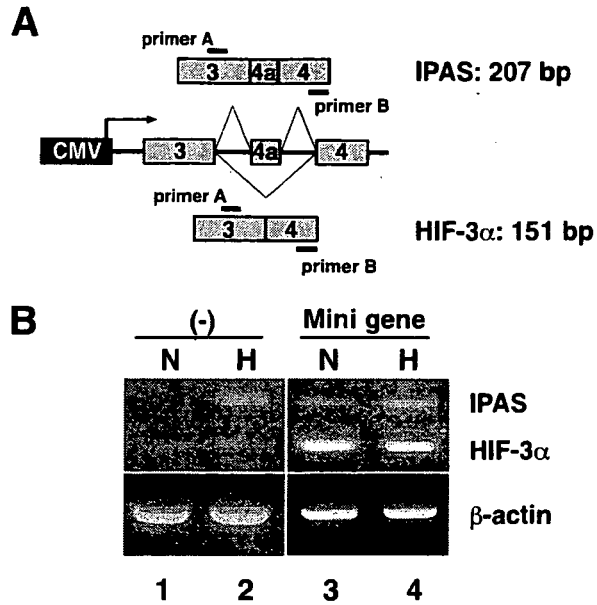

FIGURE 8. **HIF-1-mediated IPAS promoter activation and IPAS mRNA splicing can be functionally uncoupled.** *A*, schematic presentation of the structure of IPAS/HIF-3α mini-gene including exon 3, 4a, and 4. *B*, RT-PCR analysis of the expression of IPAS or HIF-3α-specific transcript. Total RNA from MBEC with or without introduction of CMV promoter-driven IPAS/HIF-3α mini-gene treated under either normoxic or hypoxic conditions was prepared. Generation of either IPAS-specific transcripts containing exon 4a or HIF-3α-specific transcripts skipping exon 4a were monitored by RT-PCR analysis using exon-specific sets of primers. β-Actin mRNA levels were monitored as a reference.

moxic and hypoxic MBEC failed to demonstrate any signals (Fig. 7, *lanes 3* and *6*). In contrast, anti-HIF-1α antibody enriched HRE-containing IPAS and VEGF genomic DNA fragments from hypoxia-exposed cells (Fig. 7, *lanes 4* and *5*), suggesting that these sequence elements were occupied by HIF-1α protein in hypoxic cells.

Hypoxia-inducible IPAS mRNA Splicing Is Observed in the Absence of HIF-1-binding Site of the IPAS Promoter—As outlined above, we have previously demonstrated that an alternative splicing mechanism is involved in hypoxia-inducible enhancement of IPAS mRNA expression (20). It has recently been suggested that promoter activation and/or transcription may be coupled with mRNA processing mechanisms including alternative splicing (26, 27). We therefore investigated a possible relationship between HIF-1-mediated IPAS promoter activation and IPAS mRNA splicing, both of which processes are induced under hypoxic conditions. To this end, we generated a cell line stably integrated with a mini-gene construct carrying exons 3, 4a, and 4 and corresponding introns of the HIF-3α/IPAS locus downstream of a constitutively active CMV promoter (Fig. 8*A*). In these cells, IPAS/HIF-3α pre-mRNA encompassing exons 3–4 is generated by the CMV promoter under normoxic conditions in an HRE-independent manner. We monitored by means of RT-PCR generation of RNA products containing either exons 3, 4, or 4a. As demonstrated in an earlier study (20), the IPAS-specific splicing product containing exon 4a is observed mainly under hypoxic conditions in the cells without introduction of the mini-gene (Fig. 8*B*, *lane 2*). In contrast, in cells stably transfected with the mini-gene, higher levels of both HIF-3α- and IPAS-type transcripts are detected under normoxic conditions (Fig. 8*B*, *lane 3*), plausibly reflecting CMV promoter-driven constitutive transcription of the gene. Moreover, when the cells carrying the mini-gene were exposed to hypoxic conditions, considerable up-regulation of the levels of the IPAS-specific splicing product was observed (Fig. 8*B*, *lane 4*). Taken together, hypoxia-inducible IPAS mRNA splicing, at least in part, can be carried out in the absence of a HIF-1-binding site in the promoter region, indicating that HIF-1 binding-mediated activation of the IPAS promoter and IPAS mRNA splicing can be functionally uncoupled.

DISCUSSION

Here we have demonstrated that IPAS, a dominant negative regulator of hypoxia-inducible transcription factors, is transcriptionally up-regulated under hypoxic conditions. HIF-1 binds to the hypoxia response element in the promoter region of the IPAS gene to mediate hypoxia-dependent activation of gene transcription, thus constituting a negative feedback regulatory loop of HIF-1-dependent gene regulation.

We have previously shown that IPAS mRNA is up-regulated in certain tissues including brain, heart, lung, and skeletal muscle of the mice exposed to hypoxic conditions (19). In such tissues of hypoxic animals, expression of IPAS mRNA dominated over the accumulation of its splicing variant HIF-3α, indicating an involvement of an alternative splicing mechanism in hypoxia-dependent augmentation of IPAS mRNA expression (20). In addition to altered mRNA splicing, we have observed by RNase protection and RT-PCR assays in the same tissues (*e.g.* heart and lung) of hypoxic mice up-regulation of transcripts initiated upstream of IPAS-specific exon 1a, suggesting that hypoxia-dependent increase of IPAS mRNA levels may also depend on IPAS promoter activation. In fact, isolation and analysis of the IPAS gene promoter by means of luciferase reporter gene assays revealed hypoxia-dependent activation of the promoter. These data suggest that two distinct hypoxia-dependent mechanisms contribute to up-regulation of IPAS

expression under hypoxic conditions, providing the cells with a finely tuned mechanism of regulation of hypoxia responsiveness. In contrast, transcription from the 5′-flanking region of the HIF-3α-specific exon 1 was not up-regulated under hypoxic conditions. Moreover, we have previously shown that HIF-3α-type splicing products were not increased in any of the examined tissues of mice exposed to hypoxia (20). These observations indicate that the central mechanism for regulation of HIF-3α expression may not involve the control of mRNA levels and thus is distinct from the mode of regulation of IPAS expression. In support of this notion, HIF-3α has been shown to be regulated at the protein level by oxygen tension via the ubiquitin-proteasomal pathway targeting the HIF degradation domain (14), which is absent in the IPAS protein. Interestingly, a previous analysis of gene expression profiles of pulmonary arterial endothelial cells demonstrated up-regulation of HIF-3α by hypoxia or by a constitutively active form of HIF-1α (28). However, the microarray analysis in the study used a probe set for HIF-3α recognizing three different isoforms of the gene products of the HIF-3α/IPAS locus, and two of those isoforms contain IPAS exon 1a-type first exon. Therefore, it is possible that the results were confounded by hypoxia-dependent up-regulation of IPAS promoter-driven transcripts. Taken together, such a variety of distinct mechanisms for regulation of the products of the HIF-3α/IPAS locus demonstrate the complexity in regulation of cellular hypoxia responsiveness via hypoxia-inducible transcription factors.

In the sequential deletion analysis of the IPAS promoter, we found a colocalization of the functional sequence mediating the hypoxia inducibility of the promoter and two classical HRE-like sequences. These sequences do not show a complete match to the conventional core HRE, A/GCGTG, found in enhancer/promoter regions of HIF-1 target genes such as the Epo or VEGF genes (22, 29, 30). However, it has been shown that some degenerative HRE-like sequence are capable of mediating hypoxia-inducible gene transcription (31, 32). In fact, sequence-specific binding by the HIF-1 complex to this hypoxia-responsive 35-nt sequence in the hypoxic cells was detected both *in vivo* and *in vitro* by ChIP assay and by EMSA, respectively. In addition, EMSA employing mutated 35-nt probes demonstrated HIF-1 binding to the proximal HRE-like sequence. Therefore, we conclude that hypoxia-dependent activation of IPAS promoter involves the HRE-like motif and the transcription factor HIF-1. In strong support of this model, expression of a constitutively active form of HIF-1α by-passed the requirement of hypoxic stimuli for activation of the IPAS promoter and resulted in an induction of reporter gene expression under normoxic conditions. Moreover, removal of the HRE-like sequence motif from the reporter construct decreased this responsiveness to constitutively active HIF-1α to activate gene expression, suggesting that the presence of both the transcriptionally active HIF-1α and the HRE-like sequence is essential for IPAS promoter activation. Since an elevation of IPAS levels leads to negative regulation of the HIF-1 function (19), we propose that HIF-1 itself participates in the negative feedback loop for regulation of hypoxia responsiveness via IPAS. In analogy to our results, it has recently been shown that HIF-1-mediated gene transcription is involved in the enhancement of HIF-1α degradation pathways, which may lead to negative regulation of HIF-1-mediated signal transduction (33–35). Interestingly, besides HIF-1α, transcription-mediated negative feedback regulation has been demonstrated for several conditionally regulated transcription; NF-κB directly activates transcription of its inhibitory molecule IκB for termination of NF-κB activity (36–38); the circadian rhythm regulator Clock/brain muscle Arnt-like factor 1 heterodimer induces another set of clock genes, Period and Cryptochrome, to form an inhibitory complex with Clock for resetting the expressed protein profile in the central clock region of the brain (39, 40), and the arylhydrocarbon receptor induces transcription of the arylhydrocarbon receptor repressor gene in certain tissues, which may lead to a modulation of their detoxification capacity in affected tissues (41). Therefore, such a mode of transcriptional feedback regulation might define an important mechanism for regulation of the fundamental physiology of higher organisms.

It has recently been proposed that transcription and RNA splicing are highly coordinated processes both at the functional and structural levels (27, 42). One well characterized example of such a mode of coordination of distinct gene regulatory mechanisms is the transcriptional coactivator PGC-1; while coactivating peroxisome proliferator-activated receptor γ target gene transcription, PGC-1 promotes splicing of the transcribed RNA. Importantly, the ability of PGC-1 to function in RNA processing appears to require its prior interaction with the promoter region of that gene (26). In a similar fashion, because hypoxic conditions recruit HIF-1 to the promoter of IPAS gene and at the same time enhance the alternative splicing of IPAS (20), one may expect a link between occupation of the promoter by HIF-1 under hypoxic condition and hypoxia-dependent augmentation of alternative splicing. In the present study, we have demonstrated in a promoter swap assay assembling the constitutively active CMV promoter in front of an IPAS mini-gene construct that hypoxia-inducible inclusion of the IPAS-specific exon 4a occurs irrespective of the specific promoter context, suggesting that HIF-1 binding to the promoter and mRNA splicing can be functionally uncoupled and may have evolved either independently or in combination with one another to increase the repertoire of a cell to respond to hypoxia. Plausibly, not only the HIF-1α-IPAS-negative feedback mechanism but also complex regulatory interactions between hypoxia-inducible transcription factors and their related molecules including target gene products may coordinately regulate transcription, RNA processing, and protein stability to finely tune cellular responses to hypoxia. It will be important both from a basic physiological and a medical point of view to elucidate in molecular detail these complex interactions of hypoxic signal transduction pathways and to examine whether certain other hypoxia target genes, in addition to HIF-3α/IPAS, are regulated by altered splicing pattern under hypoxic conditions.

REFERENCES

1. Semenza, G. L., Roth, P. H., Fang, H. M., and Wang, G. L. (1994) *J. Biol. Chem.* **269,** 23757–23763
2. Shweiki, D., Itin, A., Soffer, D., and Keshet, E. (1992) *Nature* **359,** 843–845
3. Jelkmann, W. (2003) *J. Endocrinol. Investig.* **26,** 832–837
4. Wang, G. L., and Semenza, G. L. (1995) *J. Biol. Chem.* **270,** 1230–1237
5. Ema, M., Taya, S., Yokotani, N., Sogawa, K., Matsuda, Y., and Fujii-

Kuriyama, Y. (1997) *Proc. Natl. Acad. Sci. U. S. A.* **94,** 4273–4278
6. Tian, H., Hammer, R. E., Matsumoto, A. M., Russell, D. W., and McKnight, S. L. (1998) *Genes Dev.* **12,** 3320–3324
7. Gu, Y. Z., Moran, S. M., Hogenesch, J. B., Wartman, L., and Bradfield, C. A. (1998) *Gene Expr.* **7,** 205–213
8. Maxwell, P. H., Wiesener, M. S., Chang, G. W., Clifford, S. C., Vaux, E. C., Cockman, M. E., Wykoff, C. C., Pugh, C. W., Maher, E. R., and Ratcliffe, P. J. (1999) *Nature* **399,** 271–275
9. Tanimoto, K., Makino, Y., Pereira, T., and Poellinger, L. (2000) *EMBO J.* **19,** 4298–4309
10. Masson, N., Willam, C., Maxwell, P. H., Pugh, C. W., and Ratcliffe, P. J. (2001) *EMBO J.* **20,** 5197–5206
11. Schofield, C. J., and Ratcliffe, P. J. (2004) *Nat. Rev. Mol. Cell Biol.* **5,** 343–354
12. Kaelin, W. G. (2005) *Annu. Rev. Biochem.* **74,** 115–128
13. Poellinger, L., and Johnson, R. S. (2004) *Curr. Opin. Genet. Dev.* **14,** 81–85
14. Maynard, M. A., Qi, H., Chung, J., Lee, E. H., Kondo, Y., Hara, S., Conaway, R. C., Conaway, J. W., and Ohh, M. (2003) *J. Biol. Chem.* **278,** 11032–11040
15. Carrero, P., Okamoto, K., Coumailleau, P., O'Brien, S., Tanaka, H., and Poellinger, L. (2000) *Mol. Cell Biol.* **20,** 402–415
16. Kung, A. L., Wang, S., Klco, J. M., Kaelin, W. G., and Livingston, D. M. (2000) *Nat. Med.* **6,** 1335–1340
17. Lando, D., Peet, D. J., Whelan, D. A., Gorman, J. J., and Whitelaw, M. L. (2002) *Science* **295,** 858–861
18. Safran, M., and Kaelin, W. G., Jr. (2003) *J. Clin. Investig.* **111,** 779–783
19. Makino, Y., Cao, R., Svensson, K., Bertilsson, G., Asman, M., Tanaka, H., Cao, Y., Berkenstam, A., and Poellinger, L. (2001) *Nature* **414,** 550–554
20. Makino, Y., Kanopka, A., Wilson, W. J., Tanaka, H., and Poellinger, L. (2002) *J. Biol. Chem.* **277,** 32405–32408
21. Makino, Y., Nakamura, H., Ikeda, E., Ohnuma, K., Yamauchi, K., Yabe, Y., Poellinger, L., Okada, Y., Morimoto, C., and Tanaka, H. (2003) *J. Immunol.* **171,** 6534–6540
22. Wang, G. L., and Semenza, G. L. (1993) *J. Biol. Chem.* **268,** 21513–21518
23. Hu, C. J., Wang, L. Y., Chodosh, L. A., Keith, B., and Simon, M. C. (2003) *Mol. Cell Biol.* **23,** 9361–9374
24. Leonard, M. O., Cottell, D. C., Godson, C., Brady, H. R., and Taylor, C. T. (2003) *J. Biol. Chem.* **278,** 40296–40304
25. Nakamura, H., Makino, Y., Okamoto, K., Poellinger, L., Ohnuma, K., Morimoto, C., and Tanaka, H. (2005) *J. Immunol.* **174,** 7592–7599
26. Monsalve, M., Wu, Z., Adelmant, G., Puigserver, P., Fan, M., and Spiegelman, B. M. (2000) *Mol. Cell* **6,** 307–316
27. Kornblihtt, A. R., de la Mata, M., Fededa, J. P., Munoz, M. J., and Nogues, G. (2004) *RNA* **10,** 1489–1498
28. Manalo, D. J., Rowan, A., Lavoie, T., Natarajan, L., Kelly, B. D., Ye, S. Q., Garcia, J. G., and Semenza, G. L. (2005) *Blood* **105,** 659–669
29. Semenza, G. L., Jiang, B. H., Leung, S. W., Passantino, R., Concordet, J. P., Maire, P., and Giallongo, A. (1996) *J. Biol. Chem.* **271,** 32529–32537
30. Olenyuk, B. Z., Zhang, G. J., Klco, J. M., Nickols, N. G., Kaelin, W. G., Jr., and Dervan, P. B. (2004) *Proc. Natl. Acad. Sci. U. S. A.* **101,** 16768–16773
31. Wang, R., Zhang, Y. W., Zhang, X., Liu, R., Zhang, X., Hong, S., Xia, K., Xia, J., Zhang, Z., and Xu, H. (2006) *FASEB J.* **20,** 1275–1277
32. Cormier-Regard, S., Nguyen, S. V., and Claycomb, W. C. (1998) *J. Biol. Chem.* **273,** 17787–17792
33. Aprelikova, O., Chandramouli, G. V., Wood, M., Vasselli, J. R., Riss, J., Maranchie, J. K., Linehan, W. M., and Barrett, J. C. (2004) *J. Cell Biochem.* **92,** 491–501
34. Pescador, N., Cuevas, Y., Naranjo, S., Alcaide, M., Villar, D., Landazuri, M. O., and Del Peso, L. (2005) *Biochem. J.* **390,** 189–197
35. Demidenko, Z. N., Rapisarda, A., Garayoa, M., Giannakakou, P., Melillo, G., and Blagosklonny, M. V. (2005) *Oncogene* **24,** 4829–4838
36. Ghosh, S., May, M. J., and Kopp, E. B. (1998) *Annu. Rev. Immunol.* **16,** 225–260
37. Hoffmann, A., and Baltimore, D. (2006) *Immunol. Rev.* **210,** 171–186
38. Scott, M. L., Fujita, T., Liou, H. C., Nolan, G. P., and Baltimore, D. (1993) *Genes Dev.* **7,** 1266–1276
39. Lowrey, P. L., and Takahashi, J. S. (2000) *Annu. Rev. Genet.* **34,** 533–562
40. Reppert, S. M., and Weaver, D. R. (2002) *Nature* **418,** 935–941
41. Mimura, J., Ema, M., Sogawa, K., and Fujii-Kuriyama, Y. (1999) *Genes Dev.* **13,** 20–25
42. Kornblihtt, A. R. (2005) *Curr. Opin. Cell Biol.* **17,** 262–268

THE JOURNAL OF BIOLOGICAL CHEMISTRY VOL. 282, NO. 13, pp. 10117–10131, March 30, 2007

Caveolin-1 Triggers T-cell Activation via CD26 in Association with CARMA1*[S]

Received for publication, September 27, 2006, and in revised form, January 29, 2007 Published, JBC Papers in Press, February 6, 2007, DOI 10.1074/jbc.M609157200

Kei Ohnuma[‡1,2], Masahiko Uchiyama[‡1], Tadanori Yamochi[‡], Kunika Nishibashi[‡], Osamu Hosono[‡], Nozomu Takahashi[‡], Shinichiro Kina[‡], Hirotoshi Tanaka[‡], Xin Lin[§], Nam H. Dang[¶], and Chikao Morimoto[‡3]

From the [‡]Division of Clinical Immunology, Advanced Clinical Research Center, Institute of Medical Science, University of Tokyo, 4-6-1, Shirokanedai, Minato-ku, Tokyo 108-8639, Japan, the [§]Department of Molecular and Cellular Oncology, University of Texas, M. D. Anderson Cancer Center, Houston, Texas 77030, and the [¶]Department of Hematologic Malignancies, Nevada Cancer Institute, Las Vegas, Nevada 89135

CD26 is a widely distributed 110-kDa cell surface glycoprotein with an important role in T-cell costimulation. We demonstrated previously that CD26 binds to caveolin-1 in antigen-presenting cells, and following exogenous CD26 stimulation, Tollip and IRAK-1 disengage from caveolin-1 in antigen-presenting cells. IRAK-1 is then subsequently phosphorylated to up-regulate CD86 expression, resulting in subsequent T-cell proliferation. However, it is unclear whether caveolin-1 is a costimulatory ligand for CD26 in T-cells. Using soluble caveolin-1-Fc fusion protein, we now show that caveolin-1 is the costimulatory ligand for CD26, and that ligation of CD26 by caveolin-1 induces T-cell proliferation and NF-κB activation in a T-cell receptor/CD3-dependent manner. We also demonstrated that the cytoplasmic tail of CD26 interacts with CARMA1 in T-cells, resulting in signaling events that lead to NF-κB activation. Ligation of CD26 by caveolin-1 recruits a complex consisting of CD26, CARMA1, Bcl10, and IκB kinase to lipid rafts. Taken together, our findings provide novel insights into the regulation of T-cell costimulation via the CD26 molecule.

CD26 is a 110-kDa cell surface glycoprotein with known dipeptidyl peptidase IV (DPPIV,[4] EC 3.4.14.5) activity in its extracellular domain (1–3) and is capable of cleaving N-terminal dipeptides with either L-proline or L-alanine at the penultimate position (2). CD26 activity is dependent on cell type and the microenvironment, factors that can influence its multiple biological roles (reviewed in Refs. 4–8). Although CD26 expression is enhanced following activation of resting T-cells, CD4 + $CD26^{high}$ T-cells respond maximally to recall antigens such as tetanus toxoid (9, 10). Cross-linking of CD26 and CD3 with solid-phase immobilized monoclonal antibodies (mAbs) can induce T-cell costimulation and IL-2 production by CD26 + T-cells (2, 7, 10). In addition, anti-CD26 antibody treatment of T-cells enhances tyrosine phosphorylation of signaling molecules such as CD3ζ and $p56^{lck}$ (11, 12). Moreover, DPPIV activity is required for CD26-mediated T-cell costimulation (13). CD26 may therefore have an important role in T-cell biology and overall immune function. However, the costimulatory ligand of CD26 has not yet been identified, and the proximal signaling events following CD26 engagement in T-cell remain to be determined.

In our previous study (14), we identified caveolin-1 in antigen-presenting cells (APC) as a binding protein for CD26, and we demonstrated that CD26 on activated memory T-cells directly faces caveolin-1 on tetanus toxoid-loaded monocytes in the contact area, which was revealed as the immunological synapse for T-cell-APC interaction. Moreover, we showed that residues 201–211 of CD26 along with the serine catalytic site at residue 630, which constitute a pocket structure of CD26/DPPIV, contribute to binding to caveolin-1 scaffolding domain (14). More recently, we demonstrated that caveolin-1 binds to Tollip (Toll-interacting protein) and IRAK-1 (interleukin-1 receptor associated serine/threonine kinase 1) in the membrane of tetanus toxoid-loaded monocytes, and following exogenous CD26 stimulation, Tollip and IRAK-1 disengage from caveolin-1, with IRAK-1 being subsequently phosphorylated to up-regulate CD86 expression (15). It is conceivable that the interaction of CD26 with caveolin-1 on antigen-loaded monocytes results in CD86 up-regulation, therefore enhancing the subsequent interaction of CD86 and CD28 on T-cells to induce antigen-specific T-cell proliferation and activation. However, it is unclear whether caveolin-1 itself is the costimulatory ligand for T-cell CD26.

Recent studies have demonstrated that a newly identified membrane-associated guanylate kinase-like (MAGUK) molecule, CARMA1, is required for TCR/CD3-CD28 costimulation-

* This work was supported in part by a grants-in-aid from the Ministry of Education, Science, Sports and Culture (to K. O. and C. M.) and the Ministry of Health, Labor, and Welfare, Japan (to C. M.). The costs of publication of this article were defrayed in part by the payment of page charges. This article must therefore be hereby marked "*advertisement*" in accordance with 18 U.S.C. Section 1734 solely to indicate this fact.

[S] The on-line version of this article (available at http://www.jbc.org) contains supplemental primers.

[1] Both authors contributed equally to this work.

[2] Recipient of a research grant from the Japan Rheumatism Foundation.

[3] To whom correspondence should be addressed. Tel.: 81-354-495-546; Fax: 81-354-495-448; E-mail: morimoto@ims.u-tokyo.ac.jp.

[4] The abbreviations used are: DPPIV, dipeptidyl peptidase IV; APC, antigen-presenting cells; TCR, T-cell receptor; MAGUK, membrane-associated guanylate kinase; IKK, IκB kinase; aa, amino acid; mAb, monoclonal antibody; CHAPS, 3-[(3-cholamidopropyl)dimethylammonio]-1-propanesulfonic acid; MES, 4-morpholineethanesulfonic acid; TdR, thymidine; PKC, protein kinase C; GUK, guanylate kinase; pAb, polyclonal antibody; IP, immunoprecipitation; ELISA, enzyme-linked immunosorbent assay; PMA, phorbol 12-myristate 13-acetate; siRNA, small interfering RNA; FITC, fluorescein isothiocyanate; CHO, Chinese hamster ovary; SH, Src homology; IL, interleukin; huECDSP, signal peptide from human E-cadherin; rs, recombinant soluble; RU, response units; 2ME, 2-mercaptoethanol; GFP, green fluorescent protein; SCD, scaffolding domain; cyto, cytoplasmic region of CD10.

induced NF-κB activation and functions downstream of protein kinase Cθ (PKCθ) (16–18). CARMA1, which is predominantly expressed in thymus, spleen, and peripheral blood leukocytes, contains an N-terminal caspase-recruitment domain followed by a coiled-coil domain, a PDZ domain, an SH3 domain, and a guanylate kinase (GUK)-like domain (19, 20). After TCR/CD3-CD28 costimulation or PMA-CD28 stimulation, CARMA1 is phosphorylated by PKCθ, followed by association with Bcl10 and MALT1, and recruitment of these complexes into lipid rafts (21–23). The recruitment of the CARMA1-Bcl10-MALT1 complex activates IκB kinase (IKK) through a ubiquitin-dependent pathway, leading to activation of NF-κB (24–27). However, it remains to be determined whether CARMA1 is associated with lipid rafts directly or is recruited to lipid rafts via undetermined lipid raft-interacting proteins in the immunological synapse of T-cells.

In this study, using recombinant immunoglobulin-caveolin-1 fusion proteins, we identify caveolin-1 as the costimulatory ligand for CD26, and we demonstrate that the N-terminal domain of caveolin-1 induces T-cell proliferation and cytokine production via CD26 costimulation. Furthermore, we show that CARMA1 is bound to the cytoplasmic tail of dimeric CD26 on T-cells and that this interaction of CD26 and CARMA1 plays a pivotal role in CD26-mediated T-cell costimulation. Our data hence identify a previously unknown ligand for CD26 as a costimulatory molecule while elucidating the mechanisms involved in CD26-mediated T-cell activation and differentiation.

EXPERIMENTAL PROCEDURES

Expression and Purification of Fc Proteins—For initial attempts at expression of soluble forms of Fc fusion proteins, human IgG_1 Fc cassette vector was made using pCAG-EB6-MCS vector (28, 29). The 3′ portion of this cassette vector corresponding to human Ig Cγ1 (Fcγ1) sequencing (comprising hinge + CH2 + CH3 regions) was made by PCR. All the primer information used in this study is described in the Supplemental Material. The 5′ portion of the cassette vector containing the signal peptide from human E-cadherin (huECDSP) was made by PCR. Final constructs were assembled by ligating both fragments of HindIII-Fcγ1-EcoRI and SalI-huECDSP-HindIII into SalI/EcoRI-cleaved pCAG-EB6-MCS (pCAG-EB6-huECDSP-Fcγ1). The N-terminal domain of human caveolin-1 (CavNT) was made by PCR and constructed into pCAG-EB6-huECDSP-Fcγ1 (pCAG-EB6-huECDSP-CavNT-Fcγ1). With the same methods, the N-terminal domain with deletion of the scaffolding domain (CavNTΔSCD) was made by PCR (pCAG-EB6-huECDSP-CavNTΔSCD-Fcγ1). The Fc fusion protein containing amino acids 1–10 of human CD26 cytoplasmic tail (CD26 aa1–10) was constructed in identical fashion, using the primers described in the Supplemental Material (pCAG-EB6-huECDSP-CD26 aa1–10-Fcγ1).

For expression of Fc fusion proteins, FreeStyle™ 293 expression system was used according to the manufacturer's instruction (Invitrogen). The Fc fusion proteins expressed in the culture supernatant were then purified by affinity chromatography on protein A-Sepharose (Bio-Rad) followed by size-exclusion purification on Microcon® centrifugal filter devices (Millipore), and sterilized using inner diameter 0.22-μm filter microcentrifugation tube Spin-X (Corning Glass).

Cells and Reagents—HEK293FT human embryonal kidney, Jurkat T-cell line (JKTwt), and Jurkat T-cells stably transfected with human CD26 (J.CD26wt) were grown as described previously (2, 13, 14). CARMA1-deficient Jurkat T-cell line, JPM50.6, was developed as described elsewhere (18). Human peripheral blood T-cells were purified from peripheral blood mononuclear cells using MACS Pan T-cell isolation kit II (Miltenyi), collected from healthy adult volunteers and incubated according to the methods described previously (30). Informed consent was obtained from healthy adult volunteers. Biotinylation of recombinant proteins or antibody was generated using EZ-Link™ Sulfo-NHS-LC-Biotin reagents according to the manufacturer's instruction (Pierce). Protease inhibitor mixture, phosphatase inhibitor mixture, and poly-L-lysine were from Sigma. Water-soluble digitonin was purchased from Wako Pure Chemicals Industries, Ltd.

Biacore™ Analysis of Affinity of Caveolin-1-CD26 Interaction—Experiments were carried out on a Biacore™ J (Biacore, Japan) using HBS buffer (25 mM HEPES (pH 7.4), 150 mM NaCl, 3.4 mM EDTA, 0.005% surfactant P20) supplied by the manufacturer (Biacore AB). Fcγ1, NT-Fc, or NTΔSCD-Fc was coupled in 10 mM sodium acetate (pH 5.0) to a research grade CM5 sensor chip (Biacore AB) using the amine coupling kit (Biacore AB), with an activating time of 5 min, resulting in immobilization of ~5,000–6,000 response units (RU). The surface of the chip was washed with 5 mM NaOH after coupling. NaOH (5 mM) was used also to regenerate immobilized Fcγ1, NT-Fc, or NTΔSCD-Fc chips after each experiment. Recombinant soluble CD26 (rsCD26), comprising the extracellular region of human CD26, was prepared as described previously (30, 31). rsCD26 at various concentrations (50, 25, 12.5, 6.3, 3.2, and 1.6 nM) was then injected for 120 s over immobilized Fcγ1, NT-Fc, or NTΔSCD-Fc chips. Equilibrium binding analysis was performed as described elsewhere (32), using the BIAevaluation software version 2.1 (Biacore AB).

Generating Stable Transfectants—The construct of V5-tagged full-length human CD26 (pEF6/V5-CD26wt) was made by PCR, using the primers described in the Supplemental Material. The amplified products were cloned into the pEF6/V5-His B vector (Invitrogen) at the BamHI/EcoRI site. The CD26-CD10 chimeric receptor was composed of the N-terminal cytoplasmic region of human CD10 (1–23-amino acid position) ligated to the transmembrane and extracellular regions of human CD26 (7–766-amino acid position), which were made by PCR. The construct of V5-tagged monomeric human CD26 (CD26H750E), which has histidine replacing glutamic acid as a point mutation at amino acid position 750, was made by site-directed mutagenesis method using pEF6/V5-CD26w as a template with the primers described in the Supplemental Material. After constructs were confirmed by DNA sequencing, plasmids were transfected to Jurkat T-cells using Nucleofector II device according to the manufacturer's instruction (Amaxa Biosystems). Two days after transfection of indicated plasmids, the cells were selected for blasticidin (1 μg/ml) resist-

ance for 4 weeks. Single clone cells expressing CD26wt (V5-CD26wt), CD26-CD10 (V5-CD26 + CD10 cyto), and CD26H750E were then selected using standard limiting dilution method.

For rescue experiments, the CARMA1-deficient Jurkat cell line JPM50.6 was transfected with expression vectors of CD26 and/or CARMA1. The constructs of Xpress-tagged CARMA1 and its deletion mutant (CARMA1wt, CARMA1-(1–742), or CARMA1-(1–660), respectively) were made by PCR, using primers described in the Supplemental Material. The PCR products were ligated into pcDNA4/HisMax-TOPO (Invitrogen). After constructs were confirmed by DNA sequencing, plasmids were transfected to JPM50.6 cells using the Nucleofector II device according to the manufacturer's instruction. Two days after transfection of the indicated plasmids, the cells were selected for blasticidin (1 μg/ml, for cells transfected with pEF6/V5 vectors) or Zeocin (10 μg/ml, for cells transfected with pcDNA4/HisMax vectors) resistance for 4 weeks. Single clone cells expressing CD26wt (JPM50.6/CD26wt), CARMA1wt (JPM50.6/CARMA1wt), CD26wt and CARMA1wt (JPM50.6/CD26wt + CARMA1wt), or CD26wt and CARMA1-(1–660) (JPM50.6/CD26wt + CARMA1-(1–660)) were then selected using standard limiting dilution method.

For stimulation experiments using the expression system, CHO-K1 cells were transfected with GFP-fused full-length caveolin-1 or SCD-deleted caveolin-1 expression plasmids, with the constructs being described previously (14), using Lipofectamine2000 reagent (Invitrogen). Two days after transfection of the indicated plasmids, the cells were selected for G418 (500 μg/ml) resistance for 4 weeks. Single clone cells expressing GFP and caveolin-1, detected by anti-caveolin-1 pAb (N20) recognizing the N-terminal region of caveolin-1 using flow cytometry (FACSCalibur™), were then selected using standard limiting dilution method.

Flow Cytometric Analysis—For assessment of J.CD26wt that binds biotinylated NT-Fc or NTΔSCD-Fc, 1×10^6 cells were washed in ice-cold phosphate-buffered saline and incubated with Fcγ1 and mouse Ig isotypes (1 μg/ml) to block nonspecific binding, followed by reaction with biotinylated NT-Fc or NTΔSCD-Fc (1 μg/ml), and subsequently stained with FITC-conjugated streptavidin (1:500). For blocking experiments, unlabeled mouse IgG (20 μg/ml) or unlabeled anti-CD26 mAb (20 μg/ml) was incubated with cells prior to reaction with biotinylated NT-Fc or NTΔSCD-Fc. Flow cytometric analysis of 10,000 viable cells was conducted on FACSCalibur™. Each experiment was repeated at least three times, and the results were provided in the form of a histogram or dot plots of a representative experiment.

Small Interfering RNA (siRNA) against Human CARMA1—We selected two target sequences from nucleotides +305 to +325 (ss1) and +792 to + 802 (ss2) downstream of the start codon of human CARMA1 mRNA (sense1 siRNA (ss1-siRNA), 5′ AAGAGCCCACUCGGAGAUUCUdTdT, and sense2 siRNA (ss2-siRNA), 5′ AACUGGAGCGGGAGAAUGAAAdTdT). Moreover, mis-siRNA at four nucleotides was prepared to examine nonspecific effects of siRNA duplexes (mis-siRNA, 5′ UAGUGGCCACACGGUGATTCdTdT). These selected sequences also were submitted to a BLAST search against the human genome sequence to ensure that only one gene of the human genome was targeted. siRNAs were purchased from Qiagen. Transfection of siRNA into purified T-cells were conducted using HVJ-E vector (GenomeONE™; kindly provided by Ihsihara Sangyo Kaisha Ltd.) as described previously (14). After 48 h of transfection, cell were prepared for examination.

T-cell Proliferation and IL-2 Production Assay—For T-cell proliferation assay, 1×10^5 purified T-cells were cultured in 96-well flat-bottomed plates (COSTAR) in a volume of 200 μl of AIM-V medium (Invitrogen). For solid-phase stimulation, anti-CD3 (OKT3, 0.05 μg/ml) and/or anti-CD26 mAb (5 μg/ml), anti-CD28 mAb (4B10, 5 μg/ml), or Fc fusion proteins (5 μg/ml) were bound on the plates. For stimulation with caveolin-1-transfected CHO cells, purified T-cells were cultured in the presence of soluble anti-CD3 (OKT3, 0.05 μg/ml) at 1×10^5 cells/well with varying amounts (T-cells: CHO = 800, 400, 200, 100, 50, 25:1 or no CHO cells as background control) of CHO cell transfectants. Before coculturing with T-cells, CHO transfectants were fixed with 0.05% glutaraldehyde for 30 s at room temperature, followed by washing three times with phosphate-buffered saline. T-cell proliferation was measured by [^{3}H]TdR (ICN Radiochemicals) uptake. Cells were incubated for 96 h and were pulsed with 1 μCi/well of [^{3}H]TdR, 16 h prior to harvesting onto a glass fiber filter (Wallac), and the incorporated radioactivity was quantified by a liquid scintillation counter (Wallac). For blocking experiments, cells were treated with soluble anti-CD26 mAb (1F7), anti-CD28 (4B10), or control mouse Ig (each at 20 μg/ml) before being cultured in plates coated with stimulatory antibodies and/or Fc proteins.

For IL-2 production assay using Jurkat T-cell lines, JPM50.6, or their transfectants, 5×10^5 cells/well in 200 μl of culture media were incubated at 37 °C in the presence of the indicated plate-bound antibodies and/or NT-Fc proteins. Cells were also stimulated with PMA (10 ng/ml) in anti-CD3-coated wells. After 48 h of incubation, culture supernatants were pooled from the triplicate wells and assayed for IL-2 content using Human IL-2 Biotrack Easy ELISA (Amersham Biosciences) according to the manufacturer's instruction.

Two-dimensional PAGE—For two-dimensional PAGE analysis of cytosolic proteins, Jurkat cells were lysed in TBSD buffer (50 mM Tris-HCl (pH 7.6), 150 mM NaCl, 2 mM EDTA, 0.1% digitonin, 10^2-fold diluted protease inhibitor mixture, 10^2-fold diluted phosphatase inhibitor mixture), and then an aliquot (50 μg) of lysates was subjected to two-dimensional PAGE. For pulldown by CD26 aa1–10-Fc, aliquots (1 mg) of lysates were precleared by human IgG (2 μg) and protein A-Sepharose, followed by immunoprecipitation with Fcγ1 (1 μg) or CD26 aa1–10-Fc (1 μg). Total lysates or IPs were boiled at 95 °C for 3 min, and supernatants were then resuspended in rehydration lysis buffer (RHB; 8 M urea, 2 M thiourea, 4% CHAPS, 50 mM dithiothreitol, 0.5% ZOOM carrier ampholyte (pH range 3–10) (Invitrogen), 0.002% bromphenol blue). Two-dimensional PAGE and peptide mass mapping were conducted as described previously (15).

Preparation of Lysates or Lipid Raft Fractionation, Immunoprecipitation, and Western Blotting—Stimulated or unstimulated cells were pelleted and lysed with TBSD buffer (50 mM Tris-HCl (pH 7.6), 150 mM NaCl, 2 mM EDTA, 0.1% digitonin,

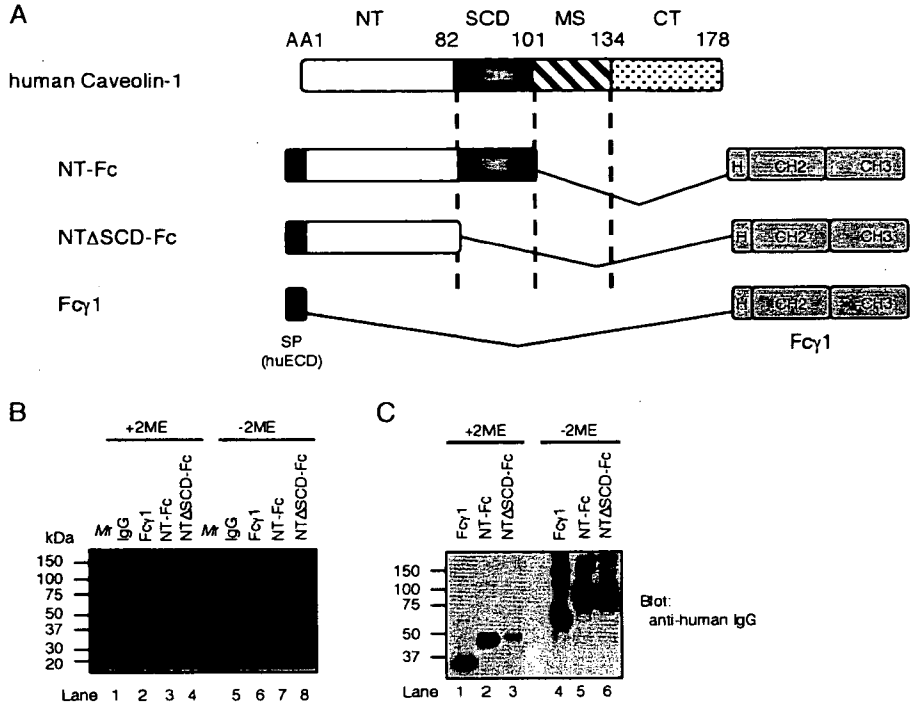

FIGURE 1. **Expression and purification of caveolin-1 human IgG_1 fusion proteins.** *A*, schematic diagrams of human caveolin-1 and its Fc fusion proteins. In human caveolin-1, aa 1–82 includes the N-terminal domain (*NT*); aa 82–101 includes the scaffolding domain (*SCD*); aa 101–134 includes membrane-spanning domain (*MS*); and aa 134–178 includes the C-terminal domain (*CT*). SP (*huECD*) depicts the signal peptide (*SP*) of human E-cadherin. At the 3′ portion, the hinge (*H*) and CH2 and CH3 domains of human IgG_1 Fc are also indicated (*Fcγ1*). *B*, expressed fusion proteins were purified as described under "Experimental Procedures." Aliquots (5 μg) of control human IgG (*lanes 1* and *5*), Fcγ1 (*lanes 2* and *6*), Fc fusion proteins of the N-terminal region of human caveolin-1 (NT-Fc) (*lanes 3* and *7*), and Fc fusion proteins of the N-terminal region with the scaffolding domain of human caveolin-1 being deleted (*NTΔSCD-Fc*) (*lanes 4* and *8*) were subjected to SDS-PAGE (5–20% acrylamide gradient gel) under reducing (*+2ME, lanes 2–4*) or nonreducing (*−2ME, lanes 5–8*) conditions. Molecular weight markers are depicted in M_r. Proteins were visualized by staining with Coomassie Brilliant Blue. *C*, aliquots (50 ng) of Fcγ1 (*lanes 1* and *4*), NT-Fc (*lanes 2* and *5*), and NTΔSCD-Fc (*lanes 3* and *6*) were subjected to SDS-PAGE (5–20% acrylamide gradient gel) under reducing (*+2ME, lanes 1–3*) or nonreducing (*−2ME, lanes 4–6*) conditions, followed by Western blot analysis, using horseradish peroxidase-conjugated anti-human IgG.

10^2-fold diluted protease inhibitor mixture (Sigma), 10^2-fold diluted phosphatase inhibitor mixture (Sigma)) and subjected to immunoprecipitation, followed by SDS-PAGE and Western blot analysis. To obtain the lipid raft fraction, purified T-cells (1×10^8) that were stimulated for 10 min with anti-CD3 alone or with anti-CD3 plus NT-Fc were lysed with 1 ml of 1% Triton X-100 and protease inhibitor mixture in ice-cold MNE buffer (25 mM MES (pH 6.5) (Sigma), 150 mM NaCl, 5 mM EDTA), and then fractionated by sucrose gradient centrifugation as described previously (33). For immunoprecipitation of the pooled lipid raft fraction, fractionated lipid rafts were lysed at 4 °C for 30 min with 1% *N*-octyl-β-D-glucoside (Nakalai Tesque) and subjected to immunoprecipitation experiment, followed by SDS-PAGE and Western blot analysis. Immunoprecipitation and Western blot analysis were conducted as described previously (14, 15, 33).

Nuclear Protein Extraction and DNA-binding Protein Assay—Nuclear extracts were prepared from Jurkat cells or transfectants stimulated as indicated, and ELISA-based DNA-binding protein assays for NF-κB p65 were performed using Mercury TransFactor kits (BD Biosciences) as described previously (14).

Statistics—Student's *t* test was used to determine whether the difference between control and sample was significant ($p < 0.05$ being significant).

RESULTS

We prepared soluble caveolin-1 protein consisting of the putative extracellular N-terminal region or the N-terminal region minus the SCD of human caveolin-1, fused with human IgG_1 Fc (NT-Fc or NTΔSCD-Fc, respectively). The schematic diagrams of the full-length human caveolin-1 protein, NT-Fc, NTΔSCD-Fc and Fcγ1 are shown in Fig. 1*A*. As shown in Fig. 1*B*, where a band of the recombinant Fc portion of human IgG_1 (Fcγ1) was observed at ~35 kDa under reducing conditions (*lane 2*), the NT-Fc and NTΔSCD-Fc proteins migrated under reducing conditions predominantly as single bands of 50 and 48 kDa, respectively (*lanes 3* and *4*). Because immunoglobulins are glycosylated post-translationally, the recombinant Fc fusion proteins produced with mammalian cells had higher a molecular weight in SDS-PAGE than as calculated from their amino acid composition (34). In nonreducing conditions, Fcγ1, NT-Fc, or NTΔSCD-Fc were observed at ~60, 100, or 90 kDa, respectively (*lanes 6–8* in Fig. 1*B*), indicating that they were expressed as a homodimer. Fcγ1, NT-Fc, and NTΔSCD-Fc were also evaluated by Western blot analysis using anti-human IgG antibody (Fig. 1*C*).

We examined whether the generated NT-Fc fusion protein binds to CD26. For this purpose, we used the Jurkat T-cell line that was stably transfected with full-length human CD26 (J.CD26wt) as described under "Experimental Procedures." As shown in Fig. 2*A*, by using lysates of J.CD26wt, CD26 was coimmunoprecipitated with NT-Fc (*lane 2*) but not with Fcγ1 (*lane 1*) nor with NTΔSCD-Fc (*lane 3*). We next evaluated binding of NT-Fc to cell surface CD26 using flow cytometry. As shown in Fig. 2*B*, cell surface CD26 of J.CD26wt was stained with anti-CD26-FITC mAb (*panel b, peak 2*) (whereas unlabeled CD26 mAb, but not control IgG, blocked staining with anti-CD26-FITC mAb (*peak 3* and *peak 4* of *panel b*). J.CD26wt was also stained with biotinylated NT-Fc followed by staining with streptavidin-conjugated FITC (*peak 2* of *panel c* in Fig. 2*B*). Staining with NT-Fc was blocked by unlabeled anti-CD26 mAb (*peak 3* of *panel c* in Fig. 2*B*) but not control IgG (*peak 4* of *panel c* in Fig. 2*B*). On the other hand, J.CD26wt was not stained with NTΔSCD-Fc (*panel d* in Fig. 2*B*). Moreover, native Jurkat

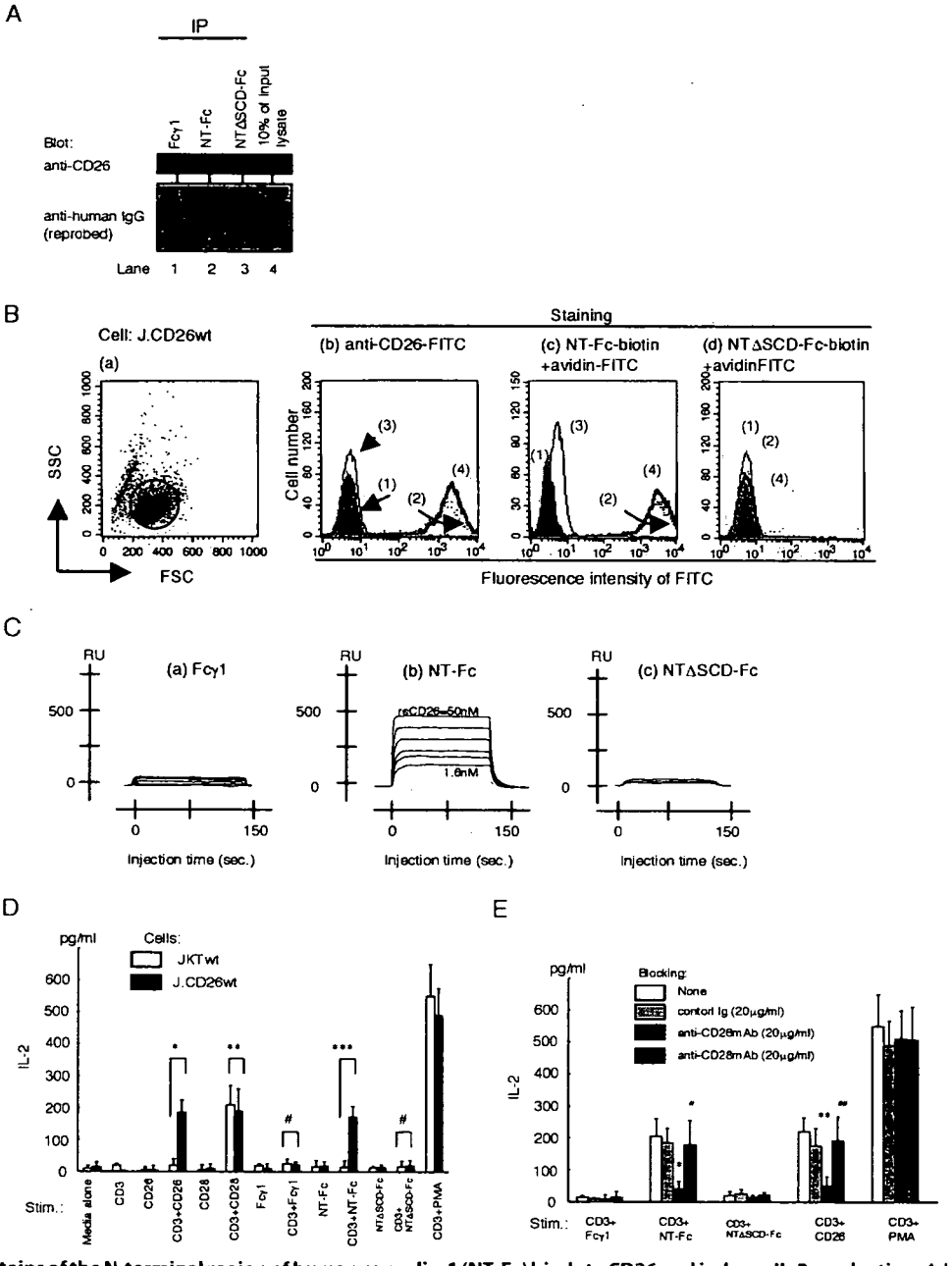

FIGURE 2. **Fc fusion proteins of the N-terminal region of human caveolin-1 (NT-Fc) binds to CD26 and induces IL-2 production.** *A*, lysates of J.CD26wt cells (500 μg) were precleared with Fcγ1 and protein A-Sepharose beads, and IP assays were conducted with Fcγ1 (*lane 1*), NT-Fc (*lane 2*), or NTΔSCD (*lane 3*) (each at 2 μg). IP complexes were then separated using 5–20% SDS-PAGE, followed by immunoblotting with anti-CD26 mAb (*upper panel*). An aliquot (50 μg) of the input lysate was also analyzed (*lane 4*). The membrane was stripped and reprobed with horseradish peroxidase-conjugated anti-human IgG (*lower panel*). Similar results were obtained in three independent experiments. *B*, J.CD26wt cells were used for binding activity of Fc fusion proteins. *Panel a*, forward and side scattergrams of the analyzed cells. *Solid circle* indicates the gated region for analysis. *Panel b*, cells were stained with FITC-conjugated control mouse IgG (*peak 1*) or FITC-conjugated anti-CD26 mAb (*peak 2*). For blocking assay, cells were first reacted with unlabeled anti-CD26 mAb (*peak 3*) or unlabeled control mouse IgG (*peak 4*), followed by staining as described in (*peak 2*). *Panel c*, cells were stained with biotinylated Fcγ1 as control (*peak 1*) or biotinylated NT-Fc (*peak 2*), followed by reaction with FITC-conjugated streptavidin. For blocking assay, cells were first reacted with unlabeled anti-CD26 mAb (*peak 3*) or unlabeled control IgG (*peak 4*), followed by staining as described in *peak 2*. *Panel d*, cells were stained with biotinylated Fcγ1 as control (*peak 1*) or biotinylated NTΔSCD-Fc (*peak 2*), followed by reaction with FITC-conjugated streptavidin. For blocking assay, cells were first reacted with unlabeled anti-CD26 mAb (*peak 3*) or unlabeled control IgG (*peak 4*), followed by staining as described in *peak 2*. All four histograms in *panel d* were stacked in the same position. *C*, measuring the affinity of Fc fusion proteins to rsCD26 by equilibrium binding. Injections of rsCD26 at 25 °C started at 50 nM and were followed by five 2-fold dilutions (50, 25, 12.5, 6.3, 3.2, and 1.6 nM), flowing over Fcγ1 (*panel a*), NT-Fc (*panel b*), or NTΔSCD-Fc (*panel c*) immobilized at a concentration of 6032, 4996, or 4852 RU, respectively. The *curves* represent total specific binding after subtraction of the background responses observed in a control flow cell. *D*, native Jurkat (JKTwt) or J.CD26wt was stimulated with immobilized antibodies and/or Fc fusion proteins (anti-CD3, 1.0 μg/ml; anti-CD28, anti-CD26, Fcγ1, NT-Fc, NTΔSCD-Fc, each at 10 μg/ml). After culturing for 48 h, culture supernatants were pooled from the triplicate wells and assayed for IL-2 content. Values shown are means ± S.E. of determinations from triplicate cultures of three independent experiments. * and *** show points of significant increase ($p < 0.05$), whereas ** and # indicate points of no significant change compared with controls. *E*, following blocking with soluble anti-CD26, anti-CD28, or control mouse IgG, J.CD26wt cells were stimulated and IL-2 was measured as described in *D*. Values shown are means ± S.E. of determinations from triplicate cultures of three independent experiments. * and ** show results of significant inhibition obtained following blocking by anti-CD26 mAb ($p < 0.05$), and # and ## show results of no significant inhibition obtained following blocking by anti-CD28 mAb.

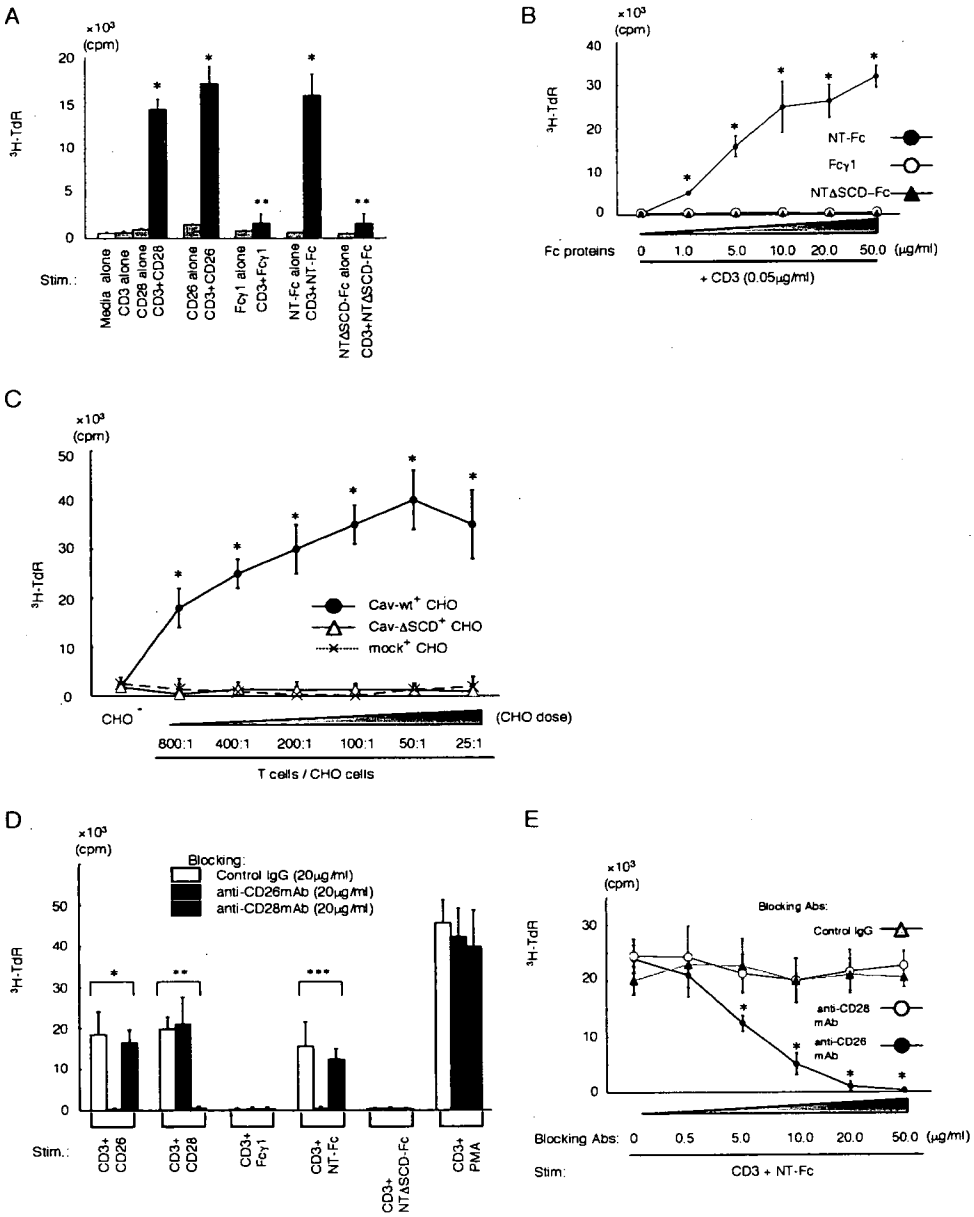

FIGURE 3. **NT-Fc is costimulatory with anti-CD3 for proliferation of peripheral blood T-cells.** *A*, purified T-cells were stimulated with immobilized antibodies and/or Fc fusion proteins (anti-CD3, 0.05 μg/ml; anti-CD28, anti-CD26, Fcγ1, NT-Fc, NTΔSCD-Fc, each at 5 μg/ml). Proliferation was measured by uptake of [^{3}H]TdR as described under "Experimental Procedures." Values shown are means ± S.E. of determinations from triplicate cultures of five independent donors. * shows points of significant increase ($p < 0.05$), whereas ** indicates points of no significant change compared with controls. *B*, purified T-cells were stimulated with immobilized Fc fusion proteins at indicated concentrations in the presence of immobilized anti-CD3 (0.05 μg/ml). Proliferation was measured as described in *A*. Values shown are means ± S.E. of determinations from triplicate cultures of five independent donors. * shows points of significant increase ($p < 0.05$) compared with control. *C*, purified T-cells were cultured in the presence of anti-CD3 (0.05 μg/ml) in solution, with varying amounts of CHO transfectants that were fixed with 0.05% glutaraldehyde. *Cav-wt$^+$ CHO*, *Cav-ΔSCD$^+$ CHO*, or *mock$^+$ CHO* represent CHO cells stably transfected with GFP-full-length caveolin-1, GFP-caveolin-1 with the scaffolding domain deleted, or GFP expressing vector, respectively. Proliferation was measured as described in *A*. Values shown are means ± S.E. of determinations from triplicate cultures of five independent donors. * shows points of significant increase ($p < 0.05$) compared with control. *D*, following blocking with soluble anti-CD26, anti-CD28, or control mouse IgG, T-cells were stimulated, and proliferation was measured as described in *A*. Values shown are means ± S.E. of determinations from triplicate cultures of five independent donors. * and *** show results of significant inhibition obtained following blocking by anti-CD26 mAb ($p < 0.05$), and ** shows results of significant inhibition obtained following blocking by anti-CD28 mAb ($p < 0.05$). *E*, following incubation and blocking with increasing doses (0, 0.5, 5.0, 10.0, 20.0, and 50 μg/ml) of soluble anti-CD26 mAbs, anti-CD28 mAbs, or control mouse IgG, T-cells were stimulated by plate-bound anti-CD3 (0.05 μg/ml) plus NT-Fc (5 μg/ml), and proliferation was measured as described in *A*. Values shown are means ± S.E. of determinations from triplicate cultures of five independent donors. * shows points of significant decrease ($p < 0.05$) compared with controls.

T-cells were not stained with anti-CD26 mAb nor with NT-Fc (data not shown). These data suggested that the soluble N-terminal domain of caveolin-1 binds to cell surface CD26 and that the SCD of caveolin-1 is necessary for binding to CD26, as shown in our previous studies (14, 15).

To investigate the properties of binding of NT-Fc to CD26, we next examined the binding affinity with the Biacore system by injecting increasing concentrations of recombinant soluble CD26 (rsCD26) over each sensor surface containing recombinant Fc fusion proteins, Fcγ1, NT-Fc, or NTΔSCD-Fc (Fig. 2*C*). rsCD26 did not bind to control recombinant Fcγ1 on a Biacore sensor chip (*panel a* in Fig. 2*C*). For each concentration of rsCD26 injected, the binding response at equilibrium was calculated by subtracting the response observed in NT-Fc, resulting in a K_d value of $\sim 2 \times 10^{-5}$ M by equilibrium binding analysis (*panel b* in Fig. 2*C*). rsCD26 did not bind to NTΔSCD-Fc on a Biacore sensor chip (*panel c* in Fig. 2*C*). These results clearly indicated that the N-terminal domain of caveolin-1 binds directly to CD26.

We next evaluated whether NT-Fc stimulation had a similar effect as anti-CD26 mAb on CD26-mediated T-cell costimulation in J.CD26wt (13). As shown in Fig. 2*D*, IL-2 production of J.CD26wt induced by plate-bound anti-CD3 plus NT-Fc was observed to be at a similar level as that induced by anti-CD3 plus anti-CD28 or by anti-CD3 plus anti-CD26 (*, **, and *** in the *bar graph*), whereas IL-2 production was not observed in JKTwt (which is CD26-negative) following stimulation by anti-CD3 plus anti-CD26 nor by anti-CD3 plus NT-Fc (* and *** in Fig. 2*D*). IL-2 production by J.CD26wt or JKTwt was not observed with the use of control recombinant Fcγ1 nor NTΔSCD-Fc (# in Fig. 2*D*). To further investigate whether the T-cell costimulatory activity of NT-Fc was exerted via CD26, blocking experiments were

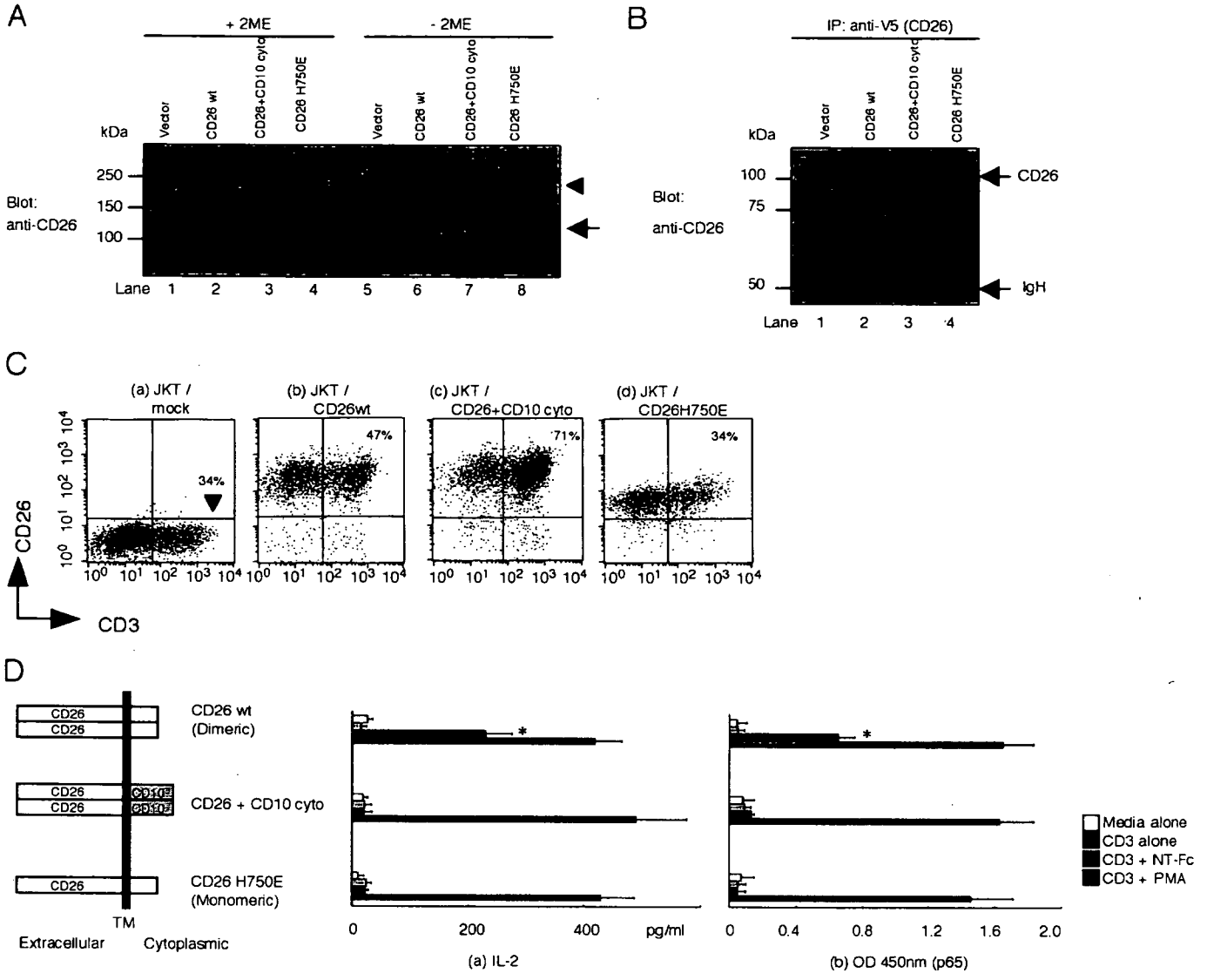

FIGURE 4. **The cytoplasmic tail of dimeric CD26 is necessary for anti-CD3 plus caveolin-1 costimulation.** *A*, Jurkat T-cells stably transfected with V5-tagged full-length CD26 (CD26wt), CD26-CD10 chimeric receptor (CD26 + CD10 cyto), or monomeric CD26 (CD26 H750E) were generated as described under "Experimental Procedures." Cell lysates were resolved in SDS-PAGE under reducing (+*2ME*) (*lanes 1–4*) or nonreducing (−*2ME*) conditions (*lanes 5–8*), and immunoblotted with anti-CD26 mAb. In nonreducing conditions, the *arrowhead* shows bands of dimeric CD26 (*lanes 6* and *7*), and the *arrow* indicates bands of monomeric CD26 (*lane 8*). *B*, cells were lysed and immunoprecipitated with anti-V5 mAb. IPs were resolved in 5–20% gradient SDS-PAGE under reducing conditions and immunoblotted with anti-CD26 mAb. *IgH* indicates immunoglobulin heavy chain. *C*, dot plots for expression of cell surface CD3 and CD26. % positive of CD3 is shown in mock vector-transfected Jurkat (*panel a*), and % positive of CD3 and CD26 is shown in other transfectants (*panels b–d*). *D*, Jurkat transfectants, which were stably transfected with full-length CD26 (CD26wt), CD26-CD10 chimeric receptor (CD26 + CD10 cyto), or CD26 containing mutation of histidine residue at amino acid 750 for glutamic acid (CD26 H750E), were stimulated with plate-bound anti-CD3 (1.0 μg/ml) in the presence or absence of plate-bound NT-Fc (10 μg/ml) or PMA (10 ng/ml). *Panel a*, following 48 h of culture, IL-2 concentration of the culture supernatant was measured by ELISA. Values shown are means ± S.E. of determinations from triplicate cultures. * shows points of significant increase ($p < 0.05$) compared with control. *Panel b*, Jurkat transfectants were stimulated as described in *panel a*, harvested for extraction of nuclear proteins, ad subjected to ELISA-based DNA-binding protein assay. Binding activity to p65 NF-κB component was revealed by absorbance value at 450 nm. Data represent mean ± S.E. from triplicate experiments. * shows a point of significant increase ($p < 0.05$).

conducted using CD26-specific mAb, which blocked binding of NT-Fc to J.CD26wt. As shown in Fig. 2*E*, IL-2 production induced by plate-bound anti-CD3 plus anti-CD26 was blocked by soluble anti-CD26 mAb but not by soluble anti-CD28 mAb (** and ##). In this experimental condition, IL-2 production induced by plate-bound anti-CD3 plus NT-Fc was blocked by soluble anti-CD26 mAb but not by soluble anti-CD28 mAb (* and # in Fig. 2*E*). Control Fγc1 or NTΔSCD-Fc did not have any T-cell costimulatory activity (Fig. 2*E*). Taken together, our results clearly indicated that caveolin-1 binds directly to CD26 and induces T-cell costimulation via CD26.

We next evaluated the ability of NT-Fc to reproduce the effects of anti-CD26 mAb on CD26-mediated T-cell costimulation (11, 35). As shown in Fig. 3*A*, T-cell proliferation induced by plate-bound anti-CD3 plus NT-Fc was observed to be at a similar level as that induced by anti-CD3 plus anti-CD28 or by anti-CD3 plus anti-CD26 (* in the *bar graph*), whereas T-cell proliferation was not observed using control recombinant Fcγ1 nor NTΔSCD-Fc (** in the *bar graph*). Moreover, T-cell costimulation induced by NT-Fc was observed in a dose-dependent manner, whereas increasing doses of Fcγ1 or NTΔSCD-Fc did not induce T-cell proliferation (Fig. 3*B*). To

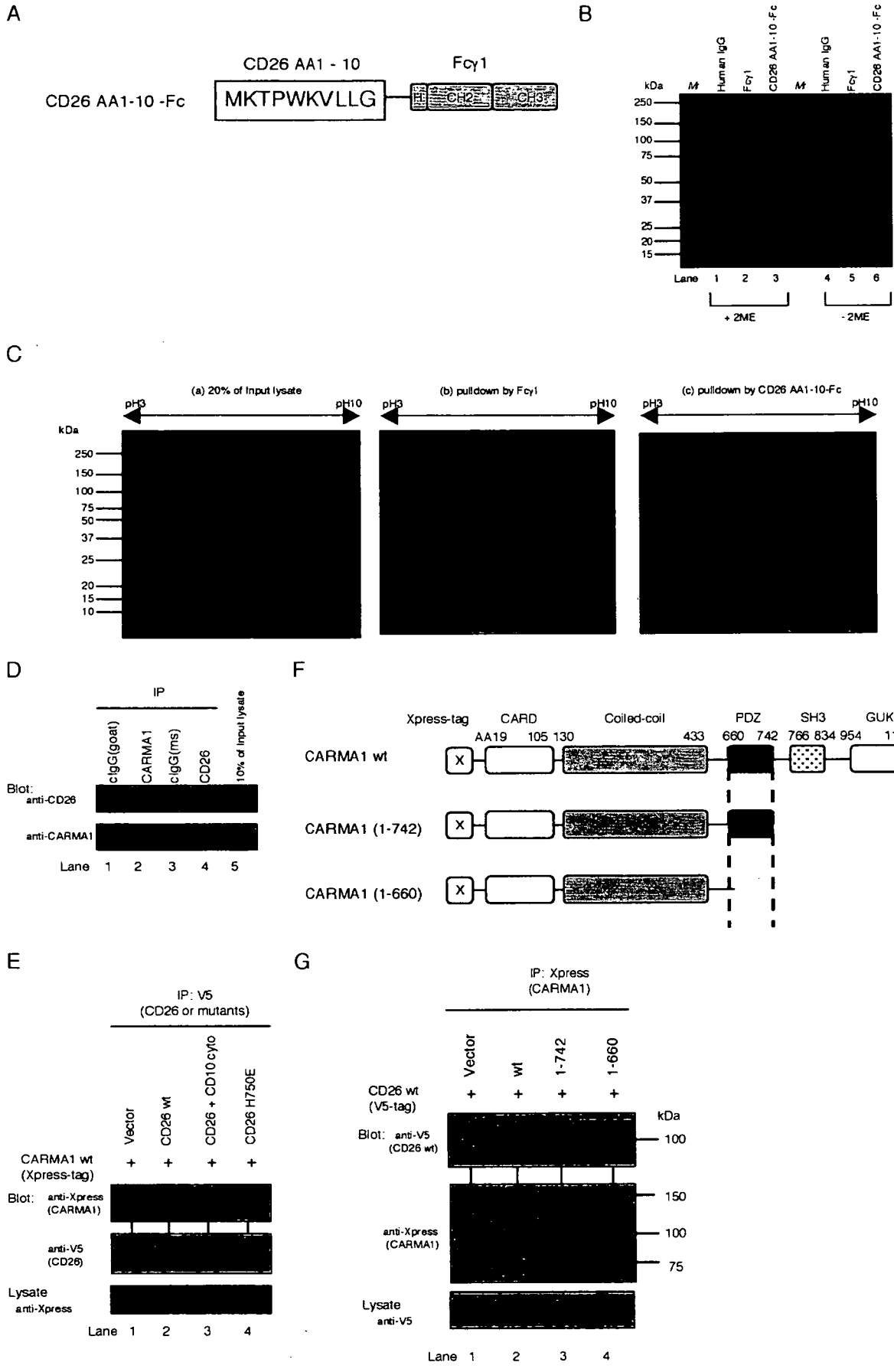
A
CD26 AA1 - 10
Fcγ1
CD26 AA1-10 -Fc
MKTPWKVLLG
H
CH2
CH3
B
kDa
M
Human IgG
Fcγ1
CD26 AA1-10 -Fc
250
150
100
75
50
37
25
20
15
Lane 1 2 3 4 5 6
+ 2ME
- 2ME
C
(a) 20% of Input lysate
(b) pulldown by Fcγ1
(c) pulldown by CD26 AA1-10-Fc
pH3
pH10
kDa
250
150
100
75
50
37
25
20
15
10
D
IP
cIgG(goat)
CARMA1
cIgG(ms)
CD26
10% of Input lysate
Blot:
anti-CD26
anti-CARMA1
Lane 1 2 3 4 5
F
Xpress-tag
CARD
Coiled-coil
PDZ
SH3
GUK
AA19 105 130 433 660 742 766 834 954 1142
CARMA1 wt
CARMA1 (1-742)
CARMA1 (1-660)
X
E
IP: V5
(CD26 or mutants)
Vector
CD26 wt
CD26 + CD10 cyto
CD26 H750E
CARMA1 wt
(Xpress-tag)
+ + + +
Blot:
anti-Xpress
(CARMA1)
anti-V5
(CD26)
Lysate
anti-Xpress
Lane 1 2 3 4
G
IP: Xpress
(CARMA1)
Vector
wt
1-742
1-660
CD26 wt
(V5-tag)
+ + + +
kDa
Blot: anti-V5
(CD26 wt)
100
150
anti-Xpress
(CARMA1)
100
75
Lysate
anti-V5
Lane 1 2 3 4

further define the costimulatory activity of caveolin-1, we prepared CHO cells stably expressing human caveolin-1. As shown in Fig. 3*C*, we then showed that Cav-wt$^+$ CHO cells expressed T-cell costimulatory activity in the presence of anti-CD3 mAb, an effect not observed with mock$^+$ CHO cells nor Cav-ΔSCD$^+$ CHO cells. The costimulatory activity of Cav-wt$^+$ CHO cells was further observed in a cell number-dependent manner (* in Fig. 3*C*).

To further investigate whether the T-cell costimulatory activity of NT-Fc is exerted via CD26, blocking experiments were conducted using CD26-specific mAb which blocked binding of NT-Fc to J.CD26 (Fig. 2*B*). As shown in Fig. 3*D*, T-cell proliferation by plate-bound anti-CD3 plus anti-CD26 was blocked by soluble anti-CD26 mAb but not by soluble anti-CD28 mAb (*). On the other hand, T-cell proliferation by plate-bound anti-CD3 plus anti-CD28 was blocked by soluble anti-CD28 mAb but not by soluble anti-CD26 mAb (** in Fig. 3*D*). In this experimental condition, T-cell proliferation by plate-bound anti-CD3 plus NT-Fc was blocked by soluble anti-CD26 mAb but not by soluble anti-CD28 mAb (*** in Fig. 3*D*). Control Fγc1 or NTΔSCD-Fc did not have any T-cell costimulatory activity (Fig. 3*D*). Moreover, the blocking effect of CD26-specific mAb on NT-Fc costimulation was observed in a dose-dependent manner (* in Fig. 3*E*), and control IgG or anti-CD28 mAb at concentrations of 0–50 μg/ml did not block NT-Fc costimulation (Fig. 3*E*). Taken together with data shown in Figs. 1–3, these data suggested that NT-Fc functionally engages CD26 and not nonspecific proteins and that caveolin-1 has a costimulatory effect on T-cell proliferation via the TCR/CD3 pathway.

The proximal signaling molecules of CD26-mediated T-cell costimulation by caveolin-1 were next determined. We first examined whether the cytoplasmic tail of CD26 is responsible for T-cell costimulation by NT-Fc in the presence of anti-CD3 mAb. For this purpose, costimulation experiments were performed on Jurkat T-cells transfected with CD26-CD10 chimeric receptor. Moreover, whereas CD26 is reported to form homodimers on cell surface (36, 37), it remains to be determined whether dimeric CD26 is responsible for CD26-mediated T-cell costimulation. Therefore, costimulation experiments were conducted using Jurkat T-cells transfected with monomeric CD26 (CD26 H750E). We first verified the Jurkat-stable transfectants, as shown in Fig. 4*A*, and CD26wt, CD26 + CD10 cyto, and CD26 H750E were detected at ~100 kDa in reducing conditions (*lanes 2–4*), bands of CD26wt and CD26 + CD10 cyto migrated at ~200 kDa (*lanes 6* and *7*), and a band of CD26 H750E migrated at 100 kDa (*lane 8*) in nonreducing conditions, indicating that CD26wt and CD26 + CD10 cyto exist as dimers, and CD26 H750E exists as monomers in the Jurkat transfectants. Moreover, as shown in Fig. 4*B*, by immunoprecipitation using anti-V5 mAb, V5-tagged CD26 was detected by anti-CD26 mAb in each transfectant (CD26wt, CD26 + CD10 cyto, or CD26 H750E) in reducing SDS-PAGE (*lanes 2–4*). Furthermore, Fig. 4*C* showed the cell surface expression of CD3 and CD26 in Jurkat transfectants. CD3 was expressed at similar intensity among transfectants (*horizontal axis* of *panels a–d* in Fig. 4*C*), whereas the intensity of cell surface CD26 expression was different between CD26wt/CD26 + CD10 cyto and CD26 H750E (*vertical axis* of *panels b–d* in Fig. 4*C*), suggesting a difference between dimeric expression and monomeric expression. CD26 was not observed in mock vector-transfected Jurkat (*JKT/mock*; *panel a* in Fig. 4*C*). Using these Jurkat transfectants, costimulation experiments by NT-Fc were conducted. As shown in Fig. 4*D*, IL-2 production was observed in CD26wt-transfected Jurkat T-cells by stimulation with anti-CD3 plus NT-Fc (* in *panel a*), but not in CD26-CD10 chimera nor in CD26 H750E-transfected Jurkat. Moreover, p65, one of NF-κB components, was activated in CD26wt-transfected Jurkat T-cells following stimulation with anti-CD3 plus NT-Fc (* in *panel b*) but not in CD26-CD10 chimera nor in CD26 H750E-transfected Jurkat. Furthermore, IL-2 production or p65 induction by stimulation with anti-CD3 plus PMA was equally observed in either of CD26wt, CD26-CD10 chimera, or CD26 H750E transfected Jurkat (*panels a* and *b* of Fig. 4*D*). These data strongly suggested that the cytoplasmic tail of dimeric CD26, but not of monomeric CD26, is responsible for T-cell costimulation by NT-Fc in the presence of anti-CD3 mAb.

Because the cytoplasmic tail of CD26 appears to play a key role for CD26-mediated T-cell costimulation as shown in Fig. 4, we next explored signaling molecules associated with the cyto-

FIGURE 5. **The cytoplasmic tail of dimeric CD26 is associated with CARMA1.** *A*, schematic diagram of Fc fusion proteins of the cytoplasmic tail of CD26 (CD26 aa1–10). *MKTPWKVLLG* depicts amino acid residues of human CD26 at 1–10 positions. At the 3′ portion, the hinge (*H*) and CH2 and CH3 domains of human IgG_1 Fc are also indicated (*Fcγ1*). *B*, expressed fusion proteins were purified as described under "Experimental Procedures." Aliquots (5 μg) of control human IgG (*lanes 1* and *4*), Fcγ1 (*lanes 2* and *5*), and CD26 aa1–10-Fc (*lanes 3* and *6*) were subjected to SDS-PAGE under reducing (+*2ME*, *lanes 1–3*) or nonreducing (−*2ME*, *lanes 4–6*) conditions. Molecular weight markers are depicted in M_r. Proteins were visualized by staining with Coomassie Brilliant Blue. *C*, an aliquot (50 μg) of Jurkat lysates was separated by two-dimensional PAGE using pH 3.0–10 nonlinear (*NL*) IPG (isoelectric focusing of proteins using immobilized pH gradient) stripped in the first dimension and 4–12% SDS-PAGE, and the gels were stained with Coomassie Brilliant Blue (*panel a*). Aliquots (1 mg) of lysates were precleared by human IgG (2 μg) and proteins A-Sepharose, followed by immunoprecipitation with Fcγ1 (1 μg) (*panel b*) or CD26 aa1–10-Fc (1 μg) (*panel c*). IPs were analyzed by two-dimensional PAGE, and six spots were clearly detected in IP complex of CD26 aa1–10-Fc (*1–6* in *panel c*). * and ** were spots of Fcγ1 and CD26-Fc (aa1–10), respectively. Similar results were obtained in five independent experiments, and the panels shown are the representative results. *D*, J.CD26wt were lysed, and IP assays were conducted with anti-CARMA1 pAb (*goat*), anti-CD26 mAb (mouse (*ms*)), or control Ig (cIgG). IP complexes as well as 10% of input lysates were then separated using SDS-PAGE, immunoblotted with indicated antibodies. Similar results were obtained in three independent experiments. *E*, 293FT cells were transiently transfected with V5-tagged full-length CD26 (CD26wt), CD26-CD10 chimeric receptor (CD26 + CD10 cyto), or CD26 containing mutation of histidine residue at amino acid 750 for glutamic acid (CD26 H750E), together with Xpress-tagged full-length CARMA1 (CARMA1wt). Cells were lysed with TBSD buffer and immunoprecipitated with anti-V5 mAb. IPs were separated using 5–20% SDS-PAGE and immunoblotted with anti-Xpress mAb (*upper panel*), followed by stripping and reprobing with anti-V5 mAb (*lower panel*). Similar results were obtained in three independent experiments. *F*, schematic diagrams of Xpress-tagged CARMA1 and its deletion mutants: CARAM1wt, Xpress-tagged full-length CARMA1; CARMA1-(1–742), Xpress-tagged CARMA1 minus the SH3 + GUK domains; CARMA1-(1–660), Xpress-tagged CARMA1 minus the PDZ + SH3 + GUK domains. *G*, 293FT cells were transiently transfected with Xpress-tagged CARMA1wt, CARMA1 with the SH3 + GUK domains deleted (residues 1–742), or CARMA1 with the PDZ + SH3 + GUK domains deleted (residues 1–660), together with V5-tagged CD26wt. Cells were lysed with TBSD buffer and immunoprecipitated with anti-Xpress mAb. IPs were separated using SDS-PAGE and immunoblotted with anti-V5 mAb (*upper panel*), followed by stripping and reprobing with anti-Xpress mAb (*lower panel*). Similar results were obtained in three independent experiments.

plasmic tail of dimeric CD26. For this purpose, we prepared Fc fusion protein containing the first 10 aa of the N-terminal residues of CD26 (CD26 aa1–10-Fc) (Fig. 5*A*). As shown in Fig. 5*B*, purified protein of CD26 aa1–10-Fc was observed at ~37 kDa in reducing conditions (*lane 3*) and at ~70 kDa in nonreducing conditions (*lane 6*), suggesting that CD26 aa1–10-Fc formed homodimers. Following pulldown by CD26 aa1–10-Fc of Jurkat T-cell lysates, molecules that interacted with CD26 aa1–10-Fc were analyzed by two-dimensional SDS-PAGE. The gel of two-dimensional PAGE using input lysates is shown in Fig. 5*C* (*panel a*). Compared with two-dimensional gel analyzing IP complex by control Fcγ1 (*panel b* in Fig. 5*C*), six spots were detected by pulldown assays with CD26 aa1–10-Fc (*panel c* in Fig. 5*C*). Using matrix-assisted laser desorption ionization time-of-flight mass spectrometry, the proteins were determined to be as follows: spot 1, epidermal cytokeratin 2 (~66 kDa); spot 2, glutamyl-tRNA synthetase (~70 kDa); spot 3, tubulin (~50 kDa); spot 4, unnamed protein (~84 kDa); spot 5, CARMA1 (~120 kDa); or spot 6, HSP70 (~55 kDa), respectively (*panel c* in Fig. 5*C*). Following five independent repeats of these experiments with similar results, the unnamed protein (spot 4) was not identified more precisely by this procedure, and the other spots other than CARMA1 were ubiquitously expressed as housekeeping proteins. Therefore, CARMA1 was identified as an interacting protein with the cytoplasmic tail of CD26 and subjected to further examination.

For further confirmation, we next performed IP studies using lysates of J.CD26wt. As shown in Fig. 5*D*, CD26 was detected in a complex of lysates coprecipitated with anti-CARMA1 pAb (*lane 2* of *upper panel*), and not coprecipitated with control goat IgG (*lane 1* of *upper panel*). Moreover, CARMA1 was detected in a complex of lysates coprecipitated with anti-CD26 mAb (*lane 4* of *lower panel* in Fig. 5*D*), and not coprecipitated with control mouse IgG (*lane 3* of *lower panel* in Fig. 5*D*). These data suggested that CARMA1 binds to CD26 in cells. To determine the binding domain between CD26 and CARMA1, coimmunoprecipitation assay was next performed using 293FT-cells cotransfected with Xpress-tagged human full-length CARMA1 (CARMA1wt) and with CD26wt, CD26 + CD10 cyto, or CD26 H750E. As shown in Fig. 5*E*, CARMA1 was coprecipitated with CD26wt (*lane 2*) but not with CD26 + CD10 cyto nor CD26 H750E (*lanes 3* and *4*). These data strongly suggested that the cytoplasmic tail and dimerization of CD26 are necessary to interact with CARMA1. We next explored the binding domain of CARMA1 to CD26. For this purpose, we prepared the C-terminal truncated deletion mutants of CARMA1 (Fig. 5*F*). As shown in Fig. 5*G*, CD26 was coprecipitated with CARMA1wt or with CARMA1-(1–742) (*lanes 2* and *3*) but not with CARMA1-(1–600) (*lane 4*), suggesting that the PDZ domain in CARMA1 was necessary for binding to CD26.

To explore the role of CARMA1 in CD26-mediated T-cell costimulation, we used CARMA1-deficient Jurkat T-cell lines JPM50.6 to conduct rescue experiments (18). As shown in Fig. 6*A*, CARMA1 and CD26 were not detected in JPM50.6 (*lane 3* of *upper* and *lower panels*), whereas CARMA1 was expressed in native Jurkat and J.CD26wt (*lanes 1* and *2* of *lower panel*), and CD26 was expressed in J.CD26wt (*lane 2* of *upper panel*) but not in native Jurkat (*lane 1* of *upper panel*). We next generated the stable transfectants using JPM50.6 as described under "Experimental Procedures." Fig. 6*B* shows that transfected Xpress-tagged CARMA1 was expressed in JPM50.6/CARMA1wt, JPM50.6/CD26wt + CARMA1wt, and JPM50.6/CD26wt + CARMA1-(1–660) and that transfected V5-tagged CD26 was expressed in JPM50.6/CD26wt, JPM50.6/CD26wt + CARMA1wt, and JPM50.6/CD26wt + CARMA1-(1–660). Fig. 6*C* shows the cell surface expression of CD3 and CD26 in JPM50.6 transfectants. CD3 was expressed at similar intensity among transfectants (*horizontal axis* of *panels a–e* in Fig. 6*C*). Although the intensity of cell surface CD26 expression was similar among JPM50.6/CD26wt, JPM50.6/CD26wt + CARMA1wt, and JPM50.6/CD26wt + CARMA1-(1–660) (*panels b, d,* and *e* in Fig. 6*C*), CD26 was not observed in JPM50.6/V (mock vector) and JPM50.6/CARMA1wt (*panels a* and *c* in Fig. 6*C*). Using these transfectants, IL-2 production and NF-κB activation assays were performed with stimulation by anti-CD3 alone or anti-CD3 plus NT-Fc. As shown in Fig. 6*D*, IL-2 production induced by anti-CD3 plus NT-Fc was clearly observed in JPM50.6/CD26wt + CARMA1 but not in JPM50.6, JPM50.6/CD26wt, JPM50.6/CARMA1, nor JPM50.6/CD26wt + CARMA1-(1–660) (*panel a*). Similarly, NF-κB activation induced by anti-CD3 plus NT-Fc was clearly observed in JPM50.6/CD26wt + CARMA1 but not in JPM50.6, JPM50.6/CD26wt, JPM50.6/CARMA1, nor JPM50.6/CD26wt+ CARMA1-(1–660) (*panel b* in Fig. 6*D*). Furthermore, IL-2 production or NF-κB activation by stimulation with anti-CD3 plus PMA was equally observed in either of the transfectants (*panels a* and *b* of Fig. 6*D*). Taken together, these results suggested that CARMA1 is necessary to exert CD26-mediated costimulation by NT-Fc.

As shown above, costimulation of CD26 is observed to be exerted via interaction of CD26 with CARMA1 in the cytoplasm in Jurkat cells. To confirm this interaction more profoundly, we performed biochemical assays using human T-cells purified from healthy adult peripheral blood mononuclear cells (APB-T-cells). For this purpose, we first conducted IP studies using lysates of APB-T-cells. As shown in Fig. 7*A*, CD26 was detected in a complex of lysates coprecipitated with anti-CARMA1 pAb (*lane 2* of *upper panel*), and not coprecipitated with control goat IgG (*lane 1* of *upper panel*). Moreover, CARMA1 was detected in a complex of lysates coprecipitated with anti-CD26 mAb (*lane 4* of *lower panel* in Fig. 7*A*), and not coprecipitated with control mouse IgG (*lane 3* of *lower panel* in Fig. 7*A*). These data suggested that CARMA1 binds to CD26 in normal T-cells.

We previously showed that nonactivated peripheral blood T-cells treated with the anti-CD26 mAb 1F7 resulted in CD26 recruitment to lipid rafts, concomitant with increased tyrosine phosphorylation of ZAP70, $p56^{lck}$, and TCRζ (33). Other investigators have reported that in the process of activation of NF-κB via CD3 costimulation, CARMA1 was recruited to lipid rafts along with Bcl10 and IKKβ (18, 25, 27, 38, 39). We therefore examined whether CD26 and CARMA1 are recruited to lipid rafts by anti-CD3 plus caveolin-1 costimulation in normal T-cells. For this purpose, using a sucrose gradient separation method, we prepared lipid raft

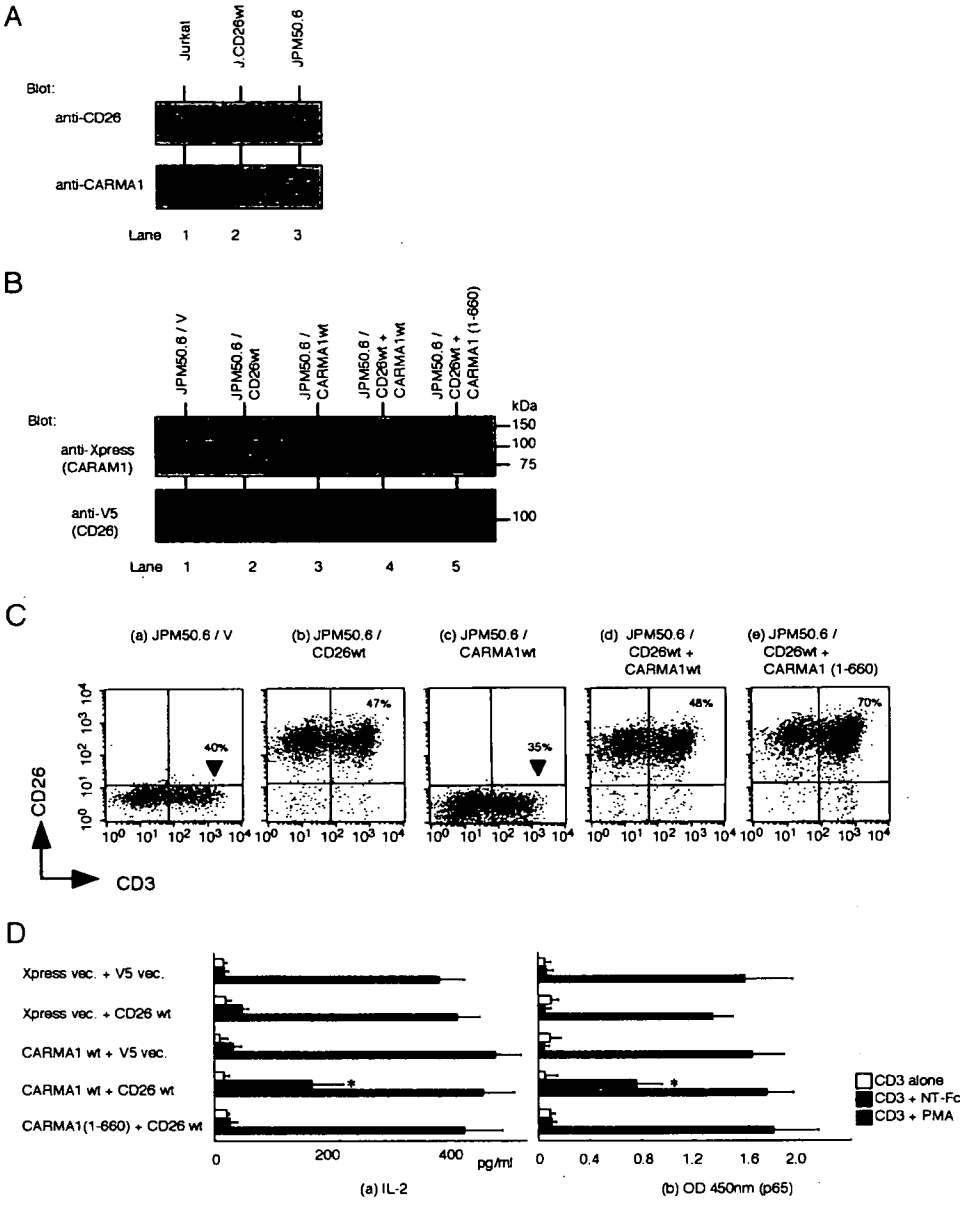

FIGURE 6. **CARMA1 is necessary for CD26-mediated costimulation by caveolin-1.** *A*, cell lysates of native Jurkat, J.CD26wt, or JPM50.6 were resolved in SDS-PAGE under reducing conditions, followed by immunoblotting with anti-CD26 mAb (*upper panel*) or anti-CARMA1 pAb (*lower panel*). *B*, JPM50.6 cells stably transfected with V5-tagged full-length CD26 (CD26wt) and/or Xpress-tagged full-length CARMA1 (CARMA1wt) or CARMA1 with the PDZ + SH3 + GUK domains deleted (CARMA1-(1–660)) were generated as described under "Experimental Procedures." Lysates were resolved in SDS-PAGE and immunoblotted with anti-Xpress mAb (CARMA1) (*upper panel*) or anti-V5 mAb (CD26) (*lower panel*). *C*, dot plots for cell surface expression of CD3 and CD26. % positive of CD3 is shown in mock vector-transfected JPM (*panel a*) and CARMA1-transfected JPM 50.6 (*panel c*), and % positive of CD3 and CD26 is shown in other transfectants (*panels b, d,* and *e*). *D*, JPM50.6 transfectants, which were described in *B*, were stimulated with plate-bound anti-CD3 in the presence or absence of plate-bound NT-Fc as described in Fig. 4*D*. *Panel a*, following 48 h of culture, IL-2 concentration of the culture supernatant was measured by ELISA. Values shown are means ± S.E. of determinations from triplicate cultures. * shows points of significant increase ($p < 0.05$) compared with control. *Panel b*, JPM50.6 transfectants were stimulated as described in *panel a* and harvested for nuclear extract. Each 5 μg of nuclear extract was subjected to ELISA-based DNA-binding protein assay. Binding activity to p65 NF-κB component was revealed by absorbance value at 450 nm. Data represent mean ± S.E. from triplicate experiments. * shows a point of significant increase ($p < 0.05$). *Xpress vec.* or *V5 vec.* depicts pcDNA4/HisMax or pEF6/V5 empty vector as a mock, respectively.

fractions of APB-T-cell lysates in the presence or absence of anti-CD3 plus NT-Fc costimulation. As shown in Fig. 7*B*, following stimulation with anti-CD3 plus NT-Fc, CD26, CARMA1, Bcl10, and IKKβ were detected in the lipid raft fractions, whereas CD26, CARMA1, Bcl10, and IKKβ were not detected in the lipid raft fractions after stimulation with anti-CD3 alone. Moreover, time course analysis revealed that CD26, CARMA1, Bcl10, and IKKβ were migrated into lipid rafts after stimulation with anti-CD3 plus NT-Fc (Fig. 7*C*), whereas CD26, CARMA1, Bcl10, and IKKβ were not detected after anti-CD3 treatment (data not shown). Furthermore, to examine whether CD26 and CARMA1 forms a complex with Bcl10 and IKKβ in lipid rafts, coprecipitation assay was performed using lipid raft fractions of APB-T-cell lysates from cells costimulated with anti-CD3 plus NT-Fc. As shown in Fig. 7*D*, CD26, CARMA1, Bcl10, and IKKβ in lipid rafts were coprecipitated with CD26 (*lane 4*), although not detected in the lysates of APB-T-cells following stimulation with anti-CD3 alone (*lane 2*). Taken together, these data indicated that ligation of CD26 by caveolin-1 recruits a complex of CARMA1, Bcl10, and IKKβ to lipid rafts in normal T-cells.

To examine the role of CARMA1 on CD26-mediated T-cell costimulation more directly, we performed siRNA experiments in freshly isolated APB-T-cells. For this purpose, we prepared two sets of specific siRNA against CARMA1 as described under "Experimental Procedures," and both of these siRNAs decreased CARMA1 expression in APB-T-cells, whereas the expression levels of CD26, TCR-β, or β-actin were not changed in the presence of control siRNA, ss1-siRNA, or ss2-siRNA (*inside box* of Fig. 7*E*). After transfection of these siRNAs into APB-T-cells, the proliferation assay was performed in the presence of anti-CD3 plus NT-Fc stimulation. As shown in Fig. 7*E*, T-cell proliferation stimulated with anti-CD3 plus NT-Fc was decreased in T-cells treated with siRNAs against CARMA1, whereas T-cell proliferation was observed in T-cells treated with control siRNA (* in Fig. 7*E*). Moreover, T-cell proliferation stimulated with anti-CD3 plus PMA was observed in either of control siRNA, ss1- or ss2-siRNA (** in Fig. 7*E*). These results suggested that CARMA1 plays an important role in signal transduction following CD26 binding to caveolin-1, leading to T-cell proliferation in normal T-cells.